Synergetic effect of electrospun PCL fiber size, orientation and plasma-modified surface chemistry on stem cell behavior

Synergetic effect of electrospun PCL fiber size, orientation and plasma-modified surface chemistry on stem cell behavior

Rouba Ghobeira[1], Charlot Philips[2], Len Liefooghe[1], Marieke Verdonck[2], Mahtab Asadian[1], Pieter Cools[1], Heidi Declercq[2], Winnok H. De Vos[3], Nathalie De Geyter[1] and Rino Morent[1]

[1]*Research Unit Plasma Technology (RUPT), Department of Applied Physics, Faculty of Architecture and Engineering, Ghent University, St-Pietersnieuwstraat 41 B4, 9000 Ghent, Belgium*

[2]*Histology and Tissue Engineering Group, Department of Basic Medical Sciences, Faculty of Medicine, Ghent University, De Pintelaan 185 (6B3), 9000 Ghent, Belgium*

[3]*Laboratory of Cell Biology and Histology, Department of Veterinary Sciences, University of Antwerp, Universiteitsplein 1, 2610 Antwerp, Belgium*

Abstract. Electrospun polymeric meshes have revolutionized the evolving tissue engineering field for their extracellular matrix mimicry. However, besides the fibrous architecture, cell-material interactions are also critically and synergistically influenced by specific surface chemical and topographical features, such as fiber size and fiber orientation. To examine these effects in detail, random polycaprolactone (PCL) fibers with average diameters of 232, 500 and 1272 nm and highly aligned fibers with diameters of 225, 482 and 1173 nm are electrospun in this work. Surface biofunctionalization is then achieved by plasma-treating the fibers using argon at medium pressure. Results reveal a significantly enhanced wettability on plasma-treated fibers due to the incorporation of oxygen-containing functionalities on their surface. A treatment time of 15 s is shown to preserve the scale and morphology of all fiber conditions. However, an extended plasma exposure starts damaging the fibers with a growing risk of drastic alterations on thicker and random fibers compared to thinner and aligned fibers. These diverse responses stem from the distinct molecular chain arrangement and crystallinity of different fiber sizes and orientations. The fibers bioresponsive properties are also profoundly investigated in this study by seeding and evaluating adipose-derived stem cells (ADSCs) performance. Plasma treatment strikingly enhances the cell metabolic activity, adhesion, proliferation and cytoplasmic remodeling on all samples. Cells adhere multi-directionally on random fibers with a gradual change from dilated and more circular to a stretched out and more elongated shape on increasing diameters. In contrast, ADSCs overextend in a bipolar and aligned fashion on aligned fibers with a tendency to attach on fewer fibers with increasing fiber diameter. A critical distinction is the cell infiltration in-between the pores of the thickest fibers. Overall, plasma-treated fibers are very promising substrates for multiple tissue engineering applications. Since the desired ADSCs behavior observed on distinct fiber size and orientation strongly depends on a specific end-application, this work constitutes a picture-perfect reference paving the way towards the optimization of the previous generation of scaffolds.

Keywords. PCL**,** fiber size, fiber orientation, plasma treatment, surface analysis, cellular behavior.

I- Introduction

Living tissues consist of multifarious populations of coordinated cells implanted in a complex 3D scaffolding, the so-called extracellular matrix (ECM). This scaffolding is mainly comprised of bioactive proteins hierarchically structured to form randomly oriented or aligned fibers having dimensions ranging from a few nanometers to a few micrometers [1-2]. The intricate ECM network provides well-defined topographical, mechanical and biochemical cues governing a broad range of cellular performances such as adhesion, proliferation, differentiation and migration [3]. Nowadays, the development of living tissue substitutes, known as tissue engineering (TE), is holding great promise to restore damaged tissue functions while overcoming the restrictions faced in conventional transplantations [4-5]. Therefore, tissue engineers are trying to understand the different physical and biochemical features ruling ECM-cell interactions in order to maximally recreate the in-vivo conditions using polymeric scaffolds [6]. First, the mimicry of the ECM fibrillary arrangement is one of the physical features guaranteeing the implant success [7]. Among several biofabrication techniques generating polymeric fibers, electrospinning is the most practical and versatile method, and is therefore the most widely used [8-9]. Secondly, appropriate mechanical cues matching those of the innate environment are of great importance to support cell growth and should be afforded by meticulously selecting a suitable base material [3]. Biodegradable aliphatic poly(α-hydroxy esters) constitute the most eminent polymer group for scaffold fabrication since in addition to their proper mechanical properties, they are also characterized by a tailorable biodegradability [10]. A remarkable supremacy is however observed for polycaprolactone (PCL) being by far the most adopted polymer in the extensive literature dealing with electrospinning. This is due to its advanced viscoelastic and rheological properties making its electrospinning adaptable and relatively easy [5, 11]. A considerable improvement in cytocompatibility was noticed when cells were grown on such PCL fibrous structures compared to 2D flat surfaces [2]. However, a fibrous morphology and a good mechanical stability are not enough to achieve the near-perfect complex biomimicry. Very specific topographical features seem to be highly characteristic of a particular end application [9]. Some authors have researched the topography size on cellular behavior and have stated that a microtopography affects the cytoskeletal structure and therefore cell morphology while a nanotopography is more involved in subcellular sensing pathways, gene expression, proliferation and differentiation [12-13]. In contrast, other studies have concluded that a nanostructured topography influences cellular morphology, adhesion and migration [2, 14]. This

discrepancy in literature suggests that the optimal topographical size is strongly dependent on the cell type and its distinctive sensing organelles. Chen et al. seeded fibroblasts on PCL fibers having diameters between 480 and 1051 nm and noticed that cell adhesion and growth kinetics decreased when increasing the fiber diameter [15]. On the other hand, Badami et al. showed that the density of osteoblastic cells tend to increase when increasing the fiber diameter from 0.14 to 2.1 μm [16]. Cells can therefore sense small size differences by forming diverse focal contact complexes depending on the frequency of available anchor points and their membrane receptors [17]. Nevertheless, the formation of focal sites is not only influenced by fiber sizes but also by their random or aligned deposition, hence the presence of anisotropic ECM alignment in some native tissues such as the heart myocardium and the inner wall of blood vessels [12, 18]. Fiber alignment provides directional cues playing a crucial role in cell shape, directed migration and regeneration enhancement of ordered tissues such as nerves and ligaments [2, 17-18]. A few cell types cultured on aligned electrospun fibers were shown to elongate and align along the axis of the fibers such as Schwann cells emulating the natural Band of Bunger structure and neurons extending directed axons for an enhanced nerve regeneration [7, 18-19]. Despite the critical influence of fiber scale and alignment on all cell types, current research is mostly focused on studying particularly neuronal cell lines on aligned fibers or other cell types on random fibers with different scales; the impact of size scaled aligned fibers is frequently neglected. Moreover, when topographical features are taken into account, the fibers biochemistry is often overlooked and vice versa [1, 20-21]. However, the structural role of the ECM components is equally complemented by their crucial and synchronic biofunctional role [5, 22]. Therefore, once the structural cues are fulfilled, a biofunctionalization should be performed by promoting the binding of growth factors and specific proteins recognized by cellular receptors in order to mediate cell affinity towards the fibers. Some authors have chosen to blend such proteins and ligands with the polymer solution prior to electrospinning [5, 23-24]. However, the electrospinning harsh conditions and the toxic solvents used can compromise the bioactive sequences of the added proteins and ligands [25-27]. Alternatively, a surface treatment introducing functional groups that subsequently attract and bind proteins can be also effective since surfaces are known to have a central role in initiating the majority of biological processes in TE applications [28-29]. Non-thermal plasma treatment is nowadays gaining considerable interest, since in contrast to the other traditional surface engineering methods, it can be highly controlled by fine-tuning all process parameters to avoid damaging of delicate nanofibrous structures [5]. It is a gas-

based technique that uniformly treats complex and porous shapes such as fibers. Moreover, the action of this solvent-free treatment is confined to a few nanometers in depth thus not altering the desired bulk properties of the base material [30-32]. By selecting a proper working gas, some authors succeeded to incorporate oxygen-containing functional groups on PCL fibers and to subsequently enhance the adhesion and proliferation of different cell types [21, 28, 33-34]. The trade-off between treatment stability/efficiency and affordability of the common low and atmospheric pressure treatments has led our research group to plasma treat PCL samples with air or argon at medium pressure [31-32, 35-36]. The surface oxygen content was successfully amplified which substantially enhanced adhesion, spreading and proliferation of adipose derived stem cells (ADSCs) [31-32]. This particular cell type is becoming the most attractive source of stem cells in TE and regenerative medicine. In opposition to other stem cells, ADSCs are abundant and easily accessible by a simple liposuction with less political and ethical issues. Despite their mesodermal origin, they are characterized by multilineage differentiation capacities involving ectodermal and mesodermal cell types [37-39]. Therefore, expanding the surface chemical study to tackle different fiber sizes and orientations will pave the way towards a critical optimization of the previously designed biomaterials to obtain scaffolds being able to reestablish the cellular equilibrium that is perturbed in-vitro. To the best of our knowledge, no study has dealt so far with the synergetic influence of PCL fiber size, orientation and surface chemistry on any cell type behavior; the few related studies found in literature were focused on only one or very rarely on two of the three factors [7, 15, 18, 33].

In view of the above, this study is divided into 2 main parts: 1-plasma activation of highly aligned and random PCL fibers with 3 different diameters each using a dielectric barrier discharge (DBD) operating in argon at medium pressure; 2-in vitro study using ADSCs. The fiber morphology and surface chemistry are characterized by means of scanning electron microscopy (SEM), X-ray photoelectron spectroscopy (XPS) and static water contact angle (WCA) goniometry. An extensive comparative study is performed by subjecting the samples to different cell tests: 3-[4,5-dimethylthiazol-2-yl]-2,5-diphenyltetrazolium (MTT) assay, live/dead staining, actin staining and dehydration followed by SEM imaging.

II- Material and methods

1- Fibers material

PCL granules (MW= 80000 g/mol), acetic acid and formic acid are purchased from Sigma-Aldrich (Belgium) and used as supplied, without any supplementary purification. Polymer solutions having concentrations of 20, 24 and 28% (w/v) are prepared by dissolving PCL in the binary solvent system formic acid/acetic acid (9:1 v/v). A complete PCL dissolution is subsequently reached by thoroughly stirring the solution at room temperature for 3 h making use of a magnetic bar.

2- Electrospinning

The Nanospinner 24 device (Inovenso, Turkey) is employed to electrospin random and aligned PCL fibers of 3 different diameters each. An electrically conductive flat cylinder (length = 1 cm, radius = 5 cm) was designed in-house to serve as metallic collector. In previous work, the new collector was extensively tested and was found to engender simultaneous electrical and mechanical effects leading to the production of highly aligned fibers at a rotational speed (RS) of 3000 rpm [40]. The generation of random fibers is also possible making use of the same collector when a speed of 100 rpm is applied. A schematic representation of the device is illustrated in Fig. 1A. During the process, the PCL solution is loaded in a syringe of 20 ml and pumped through a capillary tube to reach a copper tip. Once a solution droplet comes out of the tip, a voltage of 32 kV, safeguarding a stable jet for the 3 used PCL concentrations, is applied by a voltage-regulated DC power supply. The solution flow rate is controlled through the syringe pump and is slightly varied between 0.5 and 0.7 ml/h to ensure a stable Taylor cone over time. The fibers are deposited as non-woven mats on glass cover slips (diameter: 12 mm) taped on an aluminum sheet wrapping the collector. The process is accomplished at a temperature of 25 ± 2°C and a relative humidity of 45 ± 2% respectively. In order to obtain the desired fiber size, the polymer concentration and the tip-to-collector distance (TCD) are changed based on our previous study that profoundly analyzed the effect of each parameter on fiber diameter [40]. Table 1 displays the used electrospinning parameters and the corresponding PCL fiber diameters. SEM images of the resultant aligned and random fibers are shown in Fig. 1B. ImageJ software (National Institutes of Health, USA) is used to calculate the fiber diameter which is represented as an average diameter of 100 fibers taken from 2 different samples produced with the same electrospinning conditions. In what follows random fibers of

small, intermediate and big diameters will be referred to as R1, R2 and R3 respectively. In the same manner, aligned fibers will be denoted as A1, A2 and A3.

Table 1. Electrospinning parameters used to generate random and aligned fibers of different diameters [40].

	Random fibers			**Aligned fibers**		
Concentration (%)	20	24	28	20	20	28
TCD (cm)	20	15	15	20	15	15
RS (rpm)	100	100	100	3000	3000	3000
Averge diameter +/- standard deviation (nm)	**232.3 +/- 39.1**	**500.4 +/- 136.6**	**1272.3 +/- 382.8**	**225.6 +/- 40.9**	**482.6 +/- 183.9**	**1173.4 +/- 286.7**

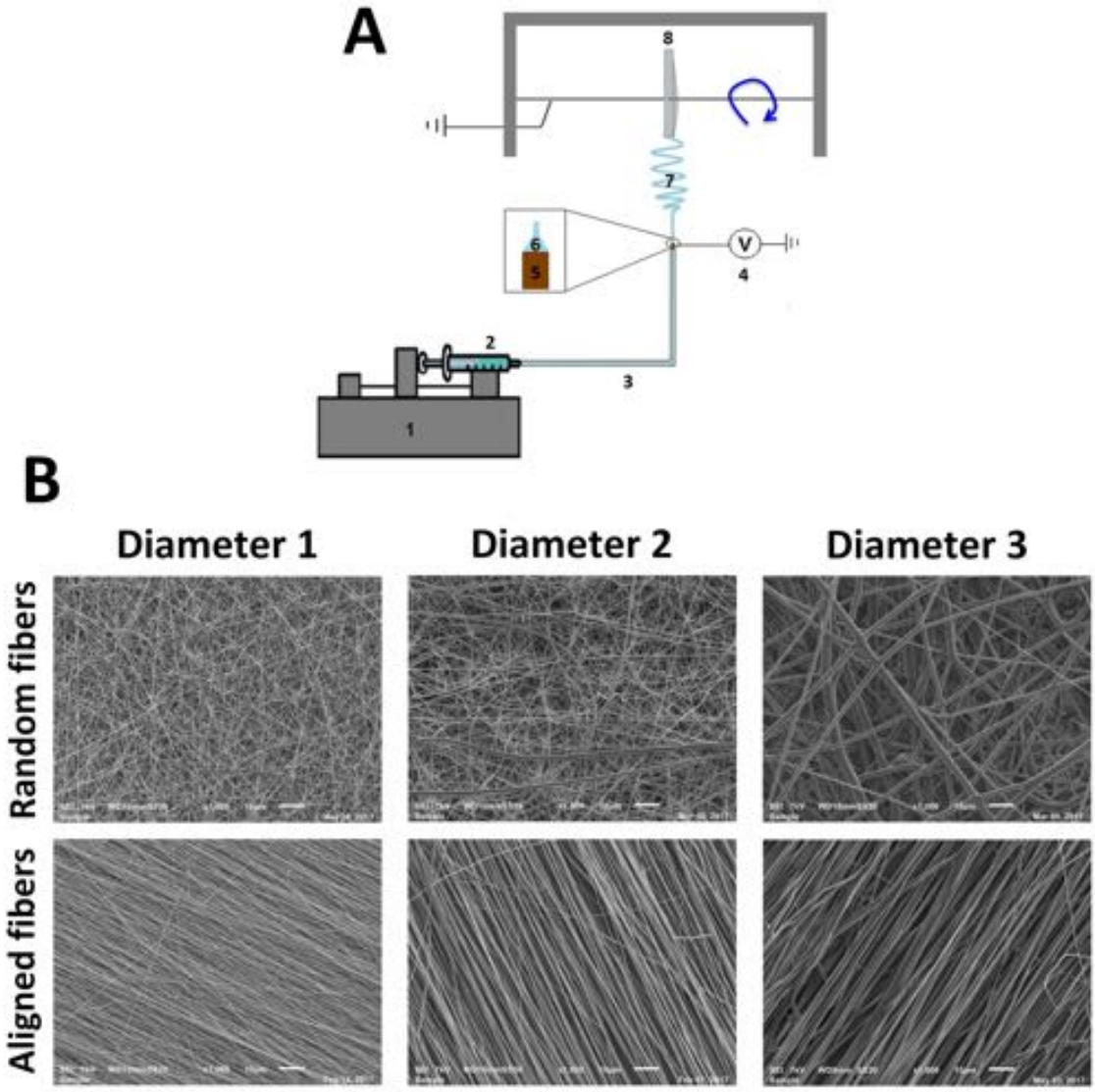

Fig. 1. Schematic illustration of the electrospinning set-up (A-1: syringe pump; 2: syringe containing the polymer solution; 3: capillary tube; 4: high voltage power supply; 5: copper tip; 6: Taylor cone; 7: polymer jet; 8: cylindrical collector) and the obtained PCL fibers (B).

3- Plasma treatment

PCL fibers are subjected to an argon plasma treatment using the parallel-plate DBD reactor depicted in Fig. 2. The setup was fully described and electrically characterized in previous work [32]. In short, the plasma chamber encompasses 2 circular copper electrodes (diameter: 4 cm) both covered by a ceramic plate (Al_2O_3, 0.7 mm thick) acting as dielectric. The upper electrode is coupled to an AC power source (frequency: 50 kHz) and the lower electrode is connected to earth, either by a capacitor C (10.4 nF) or a resistor R (50 Ω) implemented to electrically characterize the discharge. The inter-electrode gap is set to 4 mm and is supplied by a gas flow regulated by

means of a mass flow controller. The cylindrical reactor is also connected to a rotary vane pump permitting the evacuation of the plasma chamber and the subsequent pervading with a reproducible atmosphere. As a first pre-plasma step, the sample is fixed on the lower dielectric and the discharge chamber is pumped down to a pressure below 0.6 kPa. The plasma reactor is then infused with argon Alphagaz 1 (supplied from Air Liquide, Belgium) at a rate of 3 standard liters per minute (slm) until a pressure in the order of 90 kPa is established. The argon flow is retained in the chamber for 3 min to attain a uniformly spread out gas composition. Afterwards, the plasma activation step is performed at a flow rate of 1 slm and a medium pressure of 5.0 kPa with a discharge power of 1.4 W for various plasma exposure times.

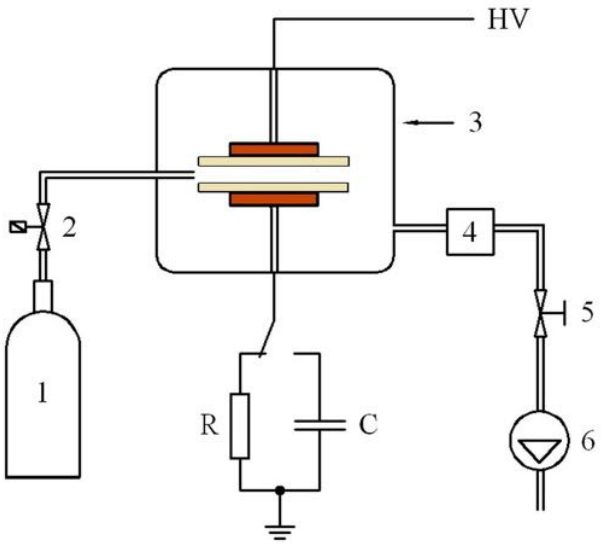

Fig. 2. Schematic illustration of the DBD set-up (1: gas cylinder; 2: mass flow controller; 3: plasma reactor; 4: pressure gauge; 5: valve; 6: pump.

4- Surface characterization techniques

a) WCA

In order to get an insight on the surface wettability of the untreated and plasma-treated PCL fibrous meshes, static WCA measurements are performed at room temperature. The commercial Krüss Easy Drop optical system (Germany, Krüss Gmbh) is used for this purpose. Distilled water drops of 2 µl are deposited on the PCL surface, after which an instantaneous determination of the drop profile is carried out using Laplace-Young curve fitting. This results in the identification of WCA values that are reported in the manuscript as the average of 4 values measured on 4 different samples of the same condition.

b) XPS

In order to assess the surface chemistry of the PCL fibrous meshes, XPS measurements are performed making use of the PHI 5000 Versaprobe II spectrometer. The samples are excited, over an area of 200 µm, with a monochromatic Al K_α X-ray source (hv = 1486.6 eV) operative at a power of 50 W. The XPS specimen chamber is continually held, during the assessment process, at a pressure of minimum 10^{-6} Pa. The detection of photoelectrons is achieved by a hemispherical analyzer tilted 45° with respect to the normal of the fibrous mesh surfaces. All binding energies are adjusted relative to 285.0 eV being the hydrocarbon component of the C1s spectrum. Survey scans, conducted on 4 randomly selected points of 2 different samples of the same condition, are recorded at a pass energy of 187.85 eV and analyzed to inspect the different surface elements. Quantification of the detected elements is carried out via Multipak software (V 9.6) using a Shirley background while considering the relative sensitivity parameters assigned by the XPS device manufacturer. Detailed high-resolution C1s spectra are also recorded using a pass energy of 23.5 eV in order to define the specific types and relative amounts of the present surface chemical bonds. Afterwards, a curve fitting of these spectra is performed using the same Multipak software. Gaussian-Lorentzian curve shapes (80-100 % Gaussian) are used during the deconvolution of the different peaks with a full width at half maximum set below 1.4 eV for each line shape.

c) SEM

In order to analyze the morphological structure of the different fiber conditions, SEM visualization is carried out and images are consequently captured at an acceleration voltage of 7 kV using the JSM-6010PLUS (JEOL, Japan) scanning electron microscope. The analyzed samples are first covered with a thin coating of fine gold particles making use of the JFC-130 autofine sputter coater (JEOL, Japan).

5- UV sterilization

Preceding cell seeding, sterilization of the fibers is required. Therefore, the samples are subjected to a UV sterilization by irradiating them using a commercially available UV lamp (Sylvania) of 15 W at a wavelength of 254 nm. A lamp–to-sample distance of 45 cm, a UV intensity of 300 µW

cm^{-2} and an exposure time of 3 h are sufficient to sterilize the fibers while avoiding fiber damage and the alteration of the induced plasma activation effects [32].

6- Adipose derived stem cells assays

a) Cell culture and seeding

Adipose tissue deriving from subcutaneous fat of Wistar rat cadavers (approved by the Ethical committee of Ghent University, Project EDC 13/14) is dissected, grinded and incubated in 0.1 % collagenase type I solution (Gibco, 17100-017) while shaking for 2 h at 37°C. The cellular suspension is then filtered making use of a cell stainer (70 µm) and centrifuged at 1200 rpm for 5 min. Thereafter, the cells are resuspended in DMEM Glutamax (Gibco™; Invitrogen) appended with 10% foetal calf serum (FCS) and 1% penicillin/streptomycin. Afterwards, the cells arecultured at 37°C in a humidified environment containing 5% CO_2. The medium is first changed after 24 h to get rid of the unattached cells and is subsequently refreshed every 3 to 4 days. ADSCs are subcultured once they get to 80-90% confluency. Cells of passage 3 are seeded on the fibrous meshes placed in a 24 well-plate at a density of 10000 cells/ 100 µl per well. More medium is added after 4 h, which is a sufficient time for the adhesion of the cells on the fibers. Tissue culture plastic (TCP) plates, serving as positive control, are also cell-seeded pursuing the same protocol. Cellular behavior is evaluated at day 1, 3 and 7 after seeding.

b) Live-dead staining (CaPi) and fluorescent microscopy

The evaluation of cell viability and attachment to the fibers is made possible by performing a live-dead staining assay. First, the supernatant is gently aspirated and the samples are rinsed with phosphate buffered saline (PBS). Afterwards, 1 ml of PBS appended with 2 µl (1 mg/ml) of calcein acetylmethoxyester purchased from Anaspec (89201) and 2 µl of propidium iodine procured by Sigma-Aldrich (P4170) is used to stain the samples. The incubation is run in the dark at room temperature for 10 min after which the samples are rinsed again with PBS and imaged by means of an Olympus IX 81 fluorescent microscope.

c) MTT assay

The quantification of the metabolic activity of ADSCs adhering and proliferating on PCL fibers is carried out by a colorimetric MTT assay. A yellow tetrazolium 3-(4,5-dimethyldiazol-2-yl)-2,5-diphenyltetrazolium bromide (MTT, Merck Promega) dye turns into purple-bleu formazan after the mitochondrial dehydrogenases of the living and metabolically active cells cause its reduction. In order to allow the occurrence of this reaction, the cell culture medium is replaced by the MTT solution (0.5 mg MTT/ml of medium), and cells are incubated for a duration of 4 h at 37°C. For the sake of dissolving the water insoluble formazan, the MTT reagent is removed and a lysis buffer, consisting of 1% Triton X-100 in isopropanol/0.4% HCl, is added and kept for 30 min at 37°C. Next, 200 µl of the solubilized formazan solution is transferred to a 96 well-plate. The absorbance of the color developed solution is assessed at 580 nm making use of a Universal microplate reader EL 800 (Biotek Instruments) spectrophotometer. The solution optical density of the PCL fibers is communicated as a ratio with respect to TCP. The reported values represent the average of 5 measured samples per condition.

d) <u>Actin cytoskeleton staining</u>

In order to visualize the actin cytoskeleton of the ADSCs and hence the cytoplasmic remodeling and morphology on different fiber conditions, a phalloidin-rhodamin staining is performed. First, the samples are fixed with a solution of 4% paraformaldehyde (PFA) for 20 min and washed 3 times with PBS. The cell permeabilization is then carried out by soaking the samples in 0.5% Triton X-100 (Sigma-Aldrich; T8787) in distilled water for 5 min, after which a washing step with PBS is again done. Next, actin cytoskeleton is stained by incubating the cells in rhodamine-phalloidin (Thermo Fisher Scientific; R415; 1/100 in PBS) for 10 min. A final wash with PBS is executed before mounting the samples with Vectashield Antifade mounting medium with DAPI (Vectorlabs; H-1200) in order to stain the nuclei.

Actin staining images are then used to quantify the cell alignment in function of the different plasma-treated fiber conditions. Fast Fourier Transform (FFT) function is applied to transform the images from real space to “frequency” space. This output representation shows grayscale pixels with a particular distribution reflecting the cell alignment on the initial actin staining images. The acquired pixel intensities are analyzed in function of the direction between 0° and 360° and then plotted only between 0° and 180° (given the symmetry in the FTT image with respect to the horizontal line). The degree of cell alignment is estimated in function of the height and the shape

of the overall distribution. The analysis is performed using the "Directionality" plugin of ImageJ analysis software.

ImageJ analysis software is also used to assess the circularity of the cell nuclei on the different fiber conditions using DAPI stained images. A circularity value of 1 designates a perfect circle. Decreasing the value and approaching 0 indicates an increasingly elongated polygon. The presented data are statistically analyzed using one-way Anova and Turkey post-hoc tests. Welch and Brown-Forsythe tests are conducted when the homogeneity of variances is violated. The significance level is fixed at $P < 0.05$

e) Cell fixation protocol for SEM imaging

The actin cytoskeleton staining is complemented with SEM imaging of the cells on the fibers that permits in addition to a detailed visualization of cell morphology, a clear scrutiny on how the ADSCs are attached, distributed and shaped on the different fiber conditions. Preceding the analysis, the cells need to be fixed and dehydrated. To do so, cells are first rinsed with PBS and incubated in a fixative solution (2.5% glutaraldehyde in 0.1 M cacodylate buffer) for 1 h. Dehydration is then performed by immersing the fibrous membranes in increasing ethanol concentrations (50%, 70%, 85%, 95% and 100%) for 10 min/immersion. The last soaking in 100% ethanol is carried out twice, with a renewed solution the second time. Thereafter, the cell-covered fibers are stored in hexamethyldisilazane (HMDS) for 10 min. HMDS is then substituted by a fresh HMDS solution that is set aside to evaporate under the fume hood. Afterwards, the samples are sputter coated with gold and imaged with SEM at an accelerating voltage of 7 kV.

III- Results and discussion

1) XPS analysis

A clear-cut evaluation of the surface elemental composition, based on XPS measurements, is first carried out on untreated fibers to check if the electrospinning process is not favoring the segregation of particular chemical functionalities on the fiber surfaces. This might induce a different surface chemistry which may be characteristic for a specific fiber orientation or fiber size since different electrospinning parameters are applied to produce each fiber condition. Nevertheless, XPS survey scan analysis shows that the surface oxygen (≈ 24%) and carbon (≈76%) content is nearly the same for all fiber conditions under study with no significant variations.

Moreover, the detected fiber surface composition, which was also perceived on spin coated PCL films, is in conformity with the PCL chemical structure contrarily to what was observed in previous studies [31]. For instance, Martins et al. electrospun PCL fibers with chloroform and N,N-dimethylformamide (DMF) as solvent mixture and found an oxygen surface percentage of only 19% [28]. Ko et al. obtained an oxygen content of 22.6% on the surface of PCL fibers electrospun using acetone [41]. A remarkably lower surface oxygen amount of 9.7% was perceived by Yan et al. on PCL fibers after electrospinning using the solvent system chloroform/methanol [42-43]. The chemical remodeling such as the enrichment of carbon on the fiber surface that occurred in former papers, is thus not taking place in the present study using acetic acid/formic acid as solvent system. The effect of electrospinning on the rearrangement of lower binding energy groups on fiber surface was already investigated for several polymers such as polylactic acid (PLA) and PLA-poly(ethylene glycol) but not for PCL [44-45]. Since different electrospinning parameters give the same surface chemistry on the different PCL fiber conditions, one can presumably conclude that the solvent system utilized to dissolve PCL is mainly influencing the chemical group remodeling which is pronounced with chloroform/methanol and not existing with acetic acid/formic acid.

After assessing the surface chemistry of the different pristine fibrous meshes, XPS measurements are also performed post-plasma treatment, in order to precisely detect the chemical modifications that are engendered. Fig. 3 depicts the oxygen percentage in function of argon plasma exposure time for the aligned and random fibers having different diameters. Although the treatment is sustained in an inert gas, a gradually ascending plasma exposure time is accompanied with a progressive increase in oxygen content attaining a maximum of approximately 30% for all fiber conditions. In return, the carbon content is proportionally decreasing as no other elements are incorporated on the surface throughout or after the plasma treatment. In order to obtain a clear insight on how oxygen-containing functionalities are implanted on PCL fibers, it is essential to elucidate the effect of the discharge gas on the different species reacting with the surface. Pure argon plasma contains several non-reactive species such as excited atoms, photons, electrons, molecules and non-reactive ions that are capable of breaking C-H and C-C chemical bonds and excite the PCL surface. Polymer radicals are thus formed which leads to the creation of a cross-linked network since these developed radicals tend to interact with other radicals of the neighboring polymer chains. Unlike air plasma treatment, argon plasma should only trigger this cross-linking and double bond formation since no chemically reactive species such as $O^{\cdot}$ and O_2

are present in theory. However, in fact, the working environment in the plasma reactor is not entirely pure. Oxygen impurities can emerge from gaseous components such as O_2 and H_2O that the plasma desorbs from the reactor inner walls during the treatment. Moreover, oxygen traces can also originate from an impure working gas or from the air lingering in the plasma chamber because of the incomplete pumping down and evacuation before running the treatment. These oxygen traces can then react with the polymer radicals induced by the plasma treatment to oxidize the surface through the implantation of certain bonds such as hydroxyl (C-O), carboxyl (O-C=O) and carbonyl (C=O). A post-treatment oxidation can also have an eminent influence on the incorporation of oxygen on the fiber surface[31, 35, 46]. The selection of argon as a discharge gas instead of air or oxygen stems from our previous study that showed PCL fiber degradation after only 10 s of air plasma exposure [32]. The high quantities of oxygen species present in air plasma tend to etch the surface and damage the fiber morphology. Currently, DBDs with advanced configurations involving for instance convexly curved electrodes are being designed for the plasma treatment of sensitive materials such as polymeric nanofibers. In contrast to the traditional DBD reactors, the newly designed reactors were shown to allow an effective air plasma surface activation of electrospun nanofibers without any significant etching and degradation [47].

The argon plasma treatment effect is saturated at an exposure time of 15s for all fiber conditions except R2 and R3 which already show a saturation of the plasma effect at 10s. This saturation is illustrated by a plateau holding on the maximum value (≈ 30%) of attained surface oxygen, signifying that a prolonged treatment time does not provoke additional chemical variations. This observation thus also shows that an argon exposure of at least 20 s is not degrading the fibers. Many studies carried out in the past have also detected an increase in oxygen content on PCL surfaces subjected to an argon plasma treatment[28, 42, 48]. However, the majority of these studies did not reach an oxygen amount of 30% especially when the initial amount is below 25%, thus highlighting the importance of the improved initial chemical properties of PCL fibers electrospun in this work.

When taking a closer look at the different fiber conditions, one can notice that although the difference in surface chemistry is negligible, the oxygen incorporation appears to develop in a slightly different trend. R2 and R3 fibers tend to incorporate a slightly higher percentage of oxygen at the different plasma treatment times with a saturation reached earlier (10 s) in comparison to the aligned and R1 fibers attaining a plasma saturation effect at 15 s. Moreover, the saturated R3 fibers

show higher standard deviations in oxygen content suggestive of a less homogeneous fibrous mesh treatment. These observations are presumably associated with the distinct arrangement of macromolecules that are forced to follow certain geometrical positions for them to fit cylindrical fibers constrained in size. The electrospinning of thin nanofibers demands a pronounced stretching of the polymer jet that also experiences additional whipping motion resulting in more aligned and densely packed molecular chains. A polymer jet undergoing less stretching and thinning ends up with the deposition of bigger fibers made up of more randomly oriented molecular chains [49-50]. The particular aligned chain assembly of thinner fibers probably makes the chemical bonds more protected by each other and less exposable to plasma. Moreover, a parallel organization of molecular chains gives rise to more Van der Waals interactions and hydrogen bonds between neighboring straight chains [51]. As a consequence, breaking surface chemical bonds to form radicals becomes harder and thus requires longer plasma exposure times. This elucidation is supported by the fact that PCL films which were previously subjected to an argon plasma treatment using the same DBD and process parameters, were saturated after a plasma exposure of only 3 s reaching a similar oxygen content. This is due to the widely exposed macromolecules on the film surface [31]. When examining aligned fibers, the difference between the 3 diameters is trifling. This is due to the fact that the fibers are subjected to enhanced mechanical forces due to a high collector rotational speed stretching the fibers even more to ensure their deposition in an aligned modus. This leads to an improved alignment and adjoining packing of the molecular chains, making the implantation of oxygen tougher in comparison to random fibers [52-53]. Moreover, aligned fibers can form more hydrogen bonds between each other as adjacent fibers are in contact along their whole length [51]. In contrast, the contact points between fibers in randomly deposited sheets are arbitrary and hence the formation of interfibrous chemical bonds is not homogenous throughout the fibrous membrane. Some locations can display more contacts where the fibrous network is dense and others can present more porous spaces and less fiber contacts, especially for the biggest fibersexhibiting larger interfibrous pores. This can possibly explain the relatively high standard deviations in oxygen content observed only for the saturated R3 fibers.

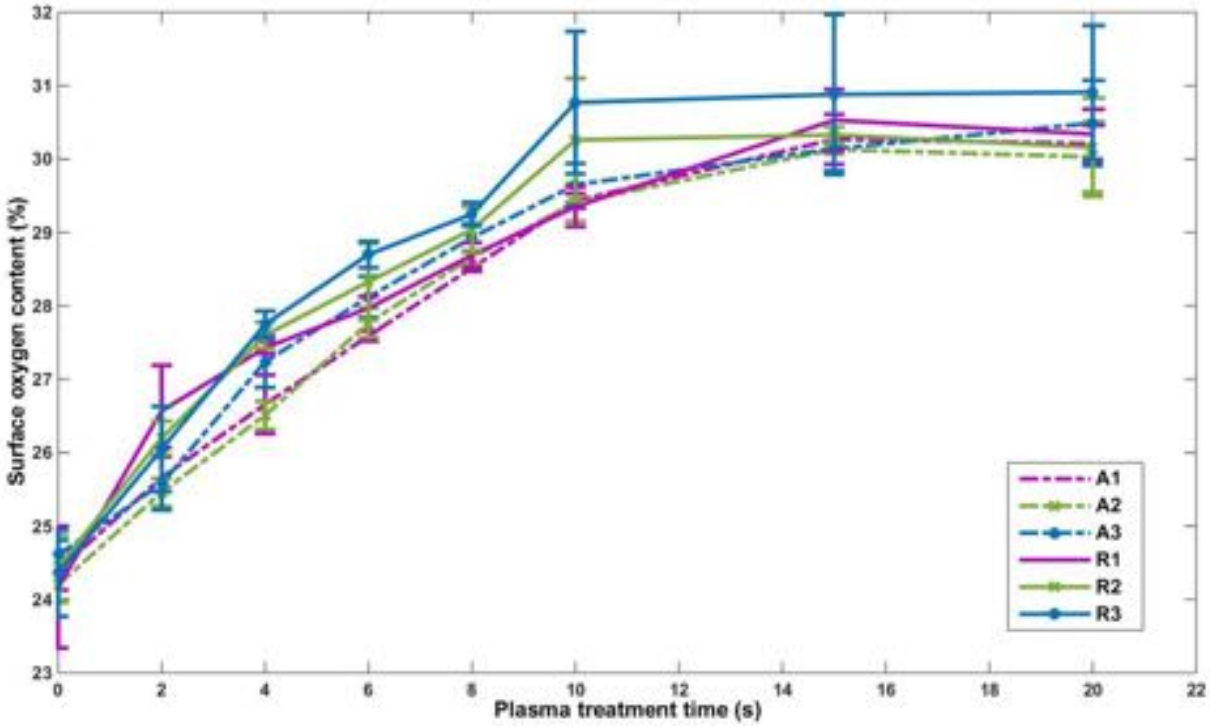

Fig. 3. Evolution of the surface oxygen percentage of PCL fibers in function of argon plasma exposure time.

For a more precise analysis of the specific types and relative amounts of the plasma induced oxygen-containing functionalities, detailed high resolution C1s curves are deconvoluted for untreated and plasma-treated fibers. Plasma treatment of 15 s which coincides with the plasma saturation effect on all fiber conditions is only considered in these measurements. According to PCL molecular structure and to literature, the C1s envelope of the polymer encompasses 3 different peaks: a peak at 285.0 eV ascribed to hydrocarbon and carbon bonds (C-H/C-C), a peak at 286.5 eV attributed to hydroxyl groups (C-O) and a peak at 289.1 eV accredited to carboxyl groups (O-C=O) [35, 54]. In fact, these peaks are identified on the untreated fibers at ratios that are similar for all fiber conditions and close to what is expected based on PCL structure (Table 2). The relative amount of the peak at 285.0 eV (≈ 69 %) is lower by 5 % than the one previously detected on PCL fibers electrospun using chloroform/methanol for instance [42-43]. This observation can validate the aforementioned assumption stating that, unlike other studies, the enrichment of methyl groups on the fiber surface over the bulk during electrospinning is not taking place in this work. After plasma treatment, the relative concentration of the 3 peaks changes noticeably but similarly on the random

and aligned fibers of different diameters. Therefore, Fig. 4 only shows the high-resolution C1s curve deconvolution of untreated and plasma-treated R1 fibers as example. An average decrease of approximately 10 % is detected for the C-C peak and increases of 5 % and 2 % are noted for the C-O and O-C=O bonds respectively. Moreover, an additional peak is distinguished at 287.7 eV corresponding to carbonyl groups (C=O) (Table 2). The decrease in C-C/C-H bonds and the incorporation of the same oxygen-containing functionalities were recurrently detected after argon plasma treatment of PCL electrospun fibers, spin-coated films and 3D printed porous scaffolds [28, 31, 35-36, 42-43]. These results confirm that argon plasma attacks C-H and C-C bonds to form radicals that finish by interacting with oxygen species instead of entirely undergoing cross-linking. Based on the quantitative data, one can notice that C-O bonds are more easily incorporated on the surface than C=O and O-C=O bonds. This was frequently observed when subjecting PCL but also other polymers such as polypropylene and PLA to argon plasma [35-36, 46, 55].

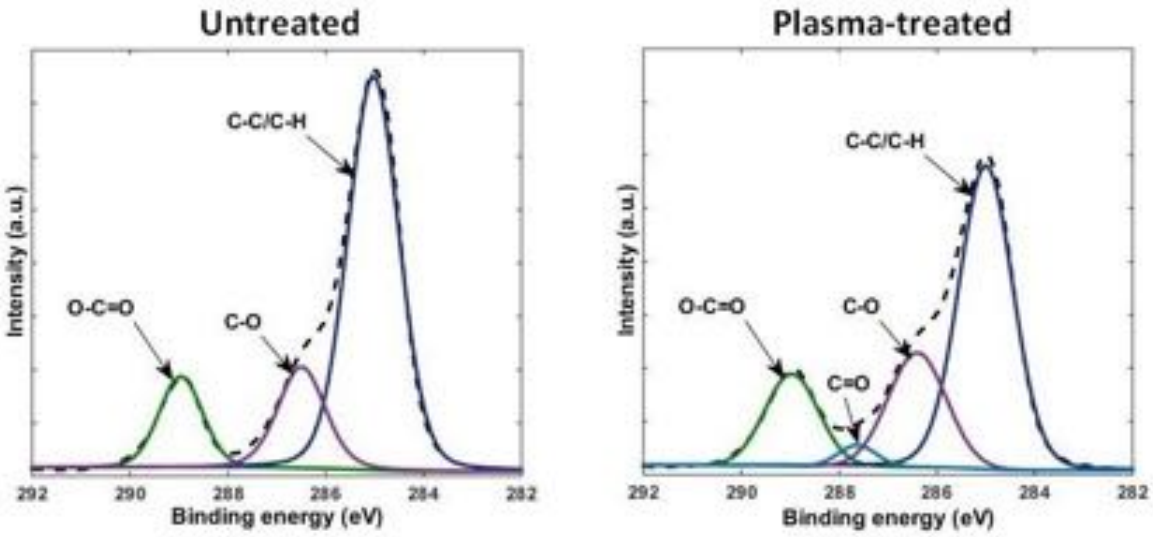

Fig. 4. C1s peak deconvolution of untreated and plasma-treated (15 s) R1 fibers.

Table 2. C1s curve fitting results of untreated and plasma-treated (15 s) PCL fibers of different conditions.

Condition		C1s curve fit (%)			
		C-C/C-H 285.0 eV	**C-O 286.5 eV**	**C=O 287.7 eV**	**O-C=O 289.1 eV**
Untreated	**R1**	69.37 +/- 0.26	17.42 +/- 0.7	0	13.19 +/- 0.12
	R2	68.40 +/- 1.26	17.15 +/- 0.56	0	14.44 +/- 0.70
	R3	68.24 +/- 0.12	17.33 +/- 0.16	0	14.43 +/- 0.14
	A1	69.08 +/- 0.82	16.96 +/- 0.82	0	13.95 +/- 0.23
	A2	68.08 +/- 0.34	17.14 +/- 0.39	0	14.77 +/- 0.38
	A3	69.46 +/- 0.33	16.13 +/- 0.56	0	14.67+/- 0.17
Plasma treatment (15 s)	**R1**	58.89 +/- 0.81	21.69 +/- 1.26	3.00 +/- 0.45	16.09 +/- 0.54
	R2	58.96 +/- 0.65	21.79 +/- 0.12	2.58 +/- 0.17	16.65 +/- 0.38
	R3	59.54 +/- 1.34	22.09 +/- 1.27	2.48 +/- 0.30	15.87 +/- 0.41
	A1	58.42 +/- 0.32	21.98 +/- 0.12	2.59 +/- 0.09	16.99 /- 0.26
	A2	59.32 +/- 0.90	21.45 +/- 0.06	2.35 +/- 0.38	16.88 +/- 0.56
	A3	58.38 +/- 0.27	22.16 +/- 0.09	2.76 +/- 0.15	16.68 +/- 0.11

2) WCA analysis

The incorporation of oxygen-containing functionalities on the plasma-treated surface meshes, clearly beheld through XPS measurements, is known to enhance surface hydrophilicity thus leading to improved protein adsorption and subsequent improved cellular adhesion. However, this phenomenon is more complex than it appears. Very specific degrees of hydrophilicity tend to have tremendously different effects on how proteins adsorb onto a surface, resulting in the finding stating that each cell type favors a particular optimal WCA [56-57]. Therefore, the hydro-properties of PCL fibers are also evaluated in the current work through WCA measurements since in addition to the surface chemistry, different mesh topographies engendered by the different fiber diameters

and orientations, are known to markedly influence the solid-liquid interface. This is first proven by the fact that, untreated random and aligned fibers with different diameters display different WCAs despite possessing the same surface chemistry. WCAs of aligned fibers gradually decrease when increasing the fiber diameter (132° for A1; 127° for A2 and 119° for A3), however, random fibers show a more irregular trend with WCAs slightly fluctuating between different diameters (134° for R1; 128° for R2 and 132° for R3). In all cases, WCA above 100° are detected, thus situating the untreated PCL fibers between the super-hydrophobic and the hydrophobic classes. In contrast, a less hydrophobic state was previously sensed on untreated PCL films that showed a WCA of 74° [31]. A markedly enhanced hydrophobicity was also observed by Dolci et al. on PLA fibers compared to PLA films revealing a WCA of 121° and 90° respectively [58]. This shows that for the same structurally hydrophobic material, a boosted hydrophobicity is perceived on fibers compared to films due to the inter-fibrous pores triggering air entrapment and thus obviating the infiltration of water [59]. The behavior of air being trapped inside pores was already described by the Cassie-Baxter equation as "heterogeneous wetting" that leads to an amplified WCA. However, in 1936, an opposite trend portrayed by the Wenzel equation was formulated on the basis stating that an increased roughness leads to a lower WCA because of water infiltration in the roughness furrows. This is denoted as "homogeneous wetting". The rivalry between homogeneous and heterogeneous wetting which aims to minimize the Gibbs energy of the system and to accordingly define the resulting WCA of a rough surface, needs therefore to be understood [60]. Homogeneous wetting seems to surpass heterogeneous wetting in case of aligned fibers since the highly packing density of the parallel fibers tends to form roughness creases instead of well delineated pores thus leading to less air entrapment. This finding is reinforced by the observed decrease in WCA on increasing mesh roughness which is dictated by broadening of the fiber diameters. Many studies have indeed depicted that the roughness of a fibrous surface proportionally follows the fiber size [61-62]. For instance, Kim et al. measured the topological properties of PCL fibrous meshes and found out a markedly increased roughness associated with an increased fiber diameter [63]. Random fibers, in contrast, do not seem to follow homogeneous wetting since the increase in fiber diameter and thus in mat roughness is not accompanied with a WCA decrease. The drop in WCA stemming from the increased roughness is most likely compensated by the enlargement of the pore size that causes more air entrapment leading to more or less similar WCAs on different fiber diameters. A balance between homogeneous and heterogeneous wetting can thus be discerned and is also

confirmed by previous studies which also obtained unchanged WCAs on PCL fibrous mats with different fiber diameters [63].

When inspecting plasma-treated samples, one can notice the pronounced effect of argon plasma causing the WCA to massively decrease to values below 25° and even attaining 0° in some cases (see Fig. 5). This effect is attributed to the polar oxygen-containing groups that are incorporated on the fibers during and after plasma exposure causing PCL to become rather hydrophilic [31]. The massive inversion from super-hydrophobic to super-hydrophilic states was also perceived in a few studies using plasma as surface functionalization method for PCL fibers [5, 28, 32-33, 42]. In contrast, a previous study conducted by our research group showed that the lowest WCA that a PCL film could reach after plasma treatment was 55° [31]. The more pronounced wettability enhancement of fibers compared to films is presumably accredited to the high fiber surface-to-volume ratio resulting in a relatively large surface area that can be treated. Moreover, when a certain threshold of chemical hydrophilicity is attained, porous structures tend to have a boosted wettability because of the penetration of water inside the pores. This is due to the fact that drops of very low tension start to overcome air entrapment by the incapability to be longer held on the surface [59]. Despite the fact that only slight differences in oxygen content occur between the different fiber conditions, differences in WCAs are plainly noticed and are portrayed as function of plasma treatment time in Fig. 5. To the best of our knowledge, no other studies have yet compared the wettability of different plasma–treated fiber sizes and orientations. For random fibers, the WCA tends to strongly decrease at shorter plasma exposure intervals for smaller fiber sizes (for R1: sudden decrease from 134° to 44° at 2 s; for R2: sudden decrease from 118° to 24° at 6 s and for R3: sudden decrease from 110° to 0° at 10 s). This is probably due to the higher surface-to-volume ratio of smaller fibers leading to a bigger surface area that is treated. This fact explains the faster penetration of water resulting in a large decrease in WCA at shorter plasma treatment times. As the fiber diameter increases, a smaller surface area is treated and the pore size increases enhancing the effect of inter-porous trapped air bubbles thus slowing down the decrease in WCA. After a certain treatment time (6 s for R2 and 10 s for R3), enough oxygen functionalities are however incorporated to overcome the effect of air entrapment and the WCA undergoes a sudden decrease. The WCA saturates at a value of 25° for R1 while it attains 0° for R2 and R3. This is due to the larger pore size in R2 and R3 causing the water drop to fully penetrate inside the mesh.

An opposite effect is observed for the aligned fibers. The WCA tends to decrease faster for larger fiber diameters (for A1: sudden decrease from 88° to 28° at 6 s; for A2: sudden decrease from 112° to 26° at 4 s and for A3: sudden decrease from 119° to 41° at 2 s). This observation is again due to the fiber alignment and high packing density resulting in a decreased porosity. Therefore, the effect of air entrapment in the pores is not influencing the WCA values to a large extend and the high packing density reduces the surface area exposed to the plasma treatment. Homogeneous wetting which is in close correlation with the mesh roughness remains the main actor of the system here. The increased roughness of larger diameters can explain the faster decrease in WCA values of A3 and the complete penetration of the water drop for the samples A2 and A3. In contrast, the decreased roughness and pore size of A1 fibers results in a WCA saturation value of 19° instead of 0°.

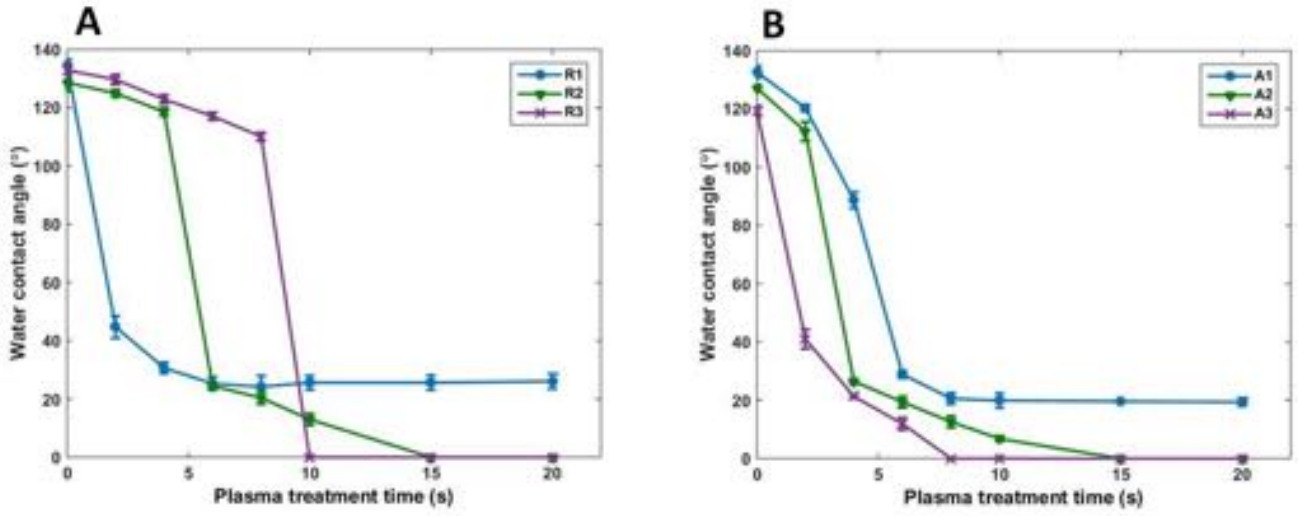

Fig. 5. Evolution of the WCA values in function of argon plasma exposure time (A: Random fibers; B: Aligned fibers).

3) SEM analysis

Besides the beneficial surface chemistry modification, an extra decisive key approving plasma treatment effectiveness is its adeptness to prevent fiber morphological damage and scale variations. To examine this, SEM images are taken after a plasma exposure time of 15 s which coincides with the chemical saturation effect of all fiber conditions. The physical effects of extended treatment times are also evaluated by visualizing the fibers exposed to plasma for 1 min (Fig. 6). All fibers

are found to retain their morphological features without any melting or flattening after 15 s of plasma treatment. Moreover, a preservation of fiber scale is detected as almost similar diameter values are obtained pre- and post-plasma treatment. Therefore, 15 s of argon plasma exposure is capable to maximally functionalize PCL fibers of different diameters and orientations without affecting their topography. Sankar et al. also perceived no deformities on PCL nano- and microfibers after subjecting them to a mild argon plasma treatment [48]. However, extending the plasma treatment time to 1 min starts to lead to some physical alterations ranging from trifling to serious deteriorations that appear distinctively on the different fiber conditions. Two phenomena damaging and antagonistically changing the fiber diameter are initiated at longer plasma stages: melting and etching. On the one hand, the melting effect is characterized by the enlargement of fiber sizes, the occurrence of melted joining points and the collapsing of neighboring fibers. It is presumably due to the electrodes that get heated at prolonged plasma ignition time because of the high energy supplied by the plasma source. On the other hand, the etching effect or surface erosion, although mainly enhanced in oxygen plasmas, is also found to be induced by argon plasma and is illustrated by fiber thinning. This phenomenon is caused by the extensive amount of chain scissions that occur in a certain treatment interval, thus dictating the generation of oligomers and the desorption of volatile compounds from the fiber surface [31]. In addition to the visual SEM inspection, both described effects are also evidenced by the large standard deviations obtained when calculating fiber diameters. A conspicuous observation that also cannot be overlooked is the different damage intensity between random and aligned fibers. Random fibers are more severely altered as melted contact points are frequently occurring (R2-R3) and fibers are collapsing (R1), thinning (R2) and severely melting (R3). Aligned fibers only show some melted point-bonded junctions (A2) and trivial fiber thinning (A3), while the thinnest fibers do not show any sign of damage. This deep scrutiny led us to the conclusion that increasing fiber size is associated with a growing risk of drastic morphological alterations. In fact, the distinct molecular chain arrangement, crystallinity and hence mechanical properties of different fiber conditions are responsible for these diverse responses to plasma. Nanofiber diameter and their resulting crystallinity are directly affected by whether a complete crystallization occurs before or after the polymer jet has reached the collector during electrospinning [50]. As already mentioned, the polymer jet experiences more whipping motion and extra elongation when generating thinner fibers. This leads, besides the formation of an aligned fibrillary structure of molecular chains, to a complete crystallization of the

jet before attaining the collector. Moreover, the rise in the crystal phase is due to the increase in inter- and intramolecular interactions that contribute to securing the molecules in a compact conformation [51]. When the polymer jet undergoes less stretching, crystallization takes place only after reaching the collector and the molecular chains accommodating thicker fibers are deposited in a misaligned non-packed lamellar structure [49-50]. First, the increased crystallinity of thinner fibers is associated with an increase in melting temperature rendering them less sensitive to heat [51]. Moreover, the locked molecules in a packed configuration have a limited degree of freedom to deform and are protecting each other from extensive chain scission. In contrast, the poor molecular arrangement, crystallinity and intermolecular interactions in larger fibers increase the molecules degree of freedom rendering them more susceptible to move and deform. Therefore, the most pronounced damage is observed for the thickest random fibers. When comparing between aligned and random fibers, some authors have noticed an increased crystallinity degree of aligned fibers [51-53]. The fiber deposition on high speed rotating collectors is shown to enhance the crystal phase owing to the extra stretching experienced by the macromolecules that concomitantly induces an additional improvement of molecular orientation. This partly explains the lower vulnerability of aligned fibers to melting and changes in their morphology. Furthermore, the decreased porosity of aligned fibers, together with the interfibrous chemical bonds along their length, strengthen their resilience against deformation.

Based on the obtained results, a plasma exposure time of 15 s is adopted in the following experiments as this exposure time is sufficient to improve the surface chemistry while maintaining an ECM-like appearance.

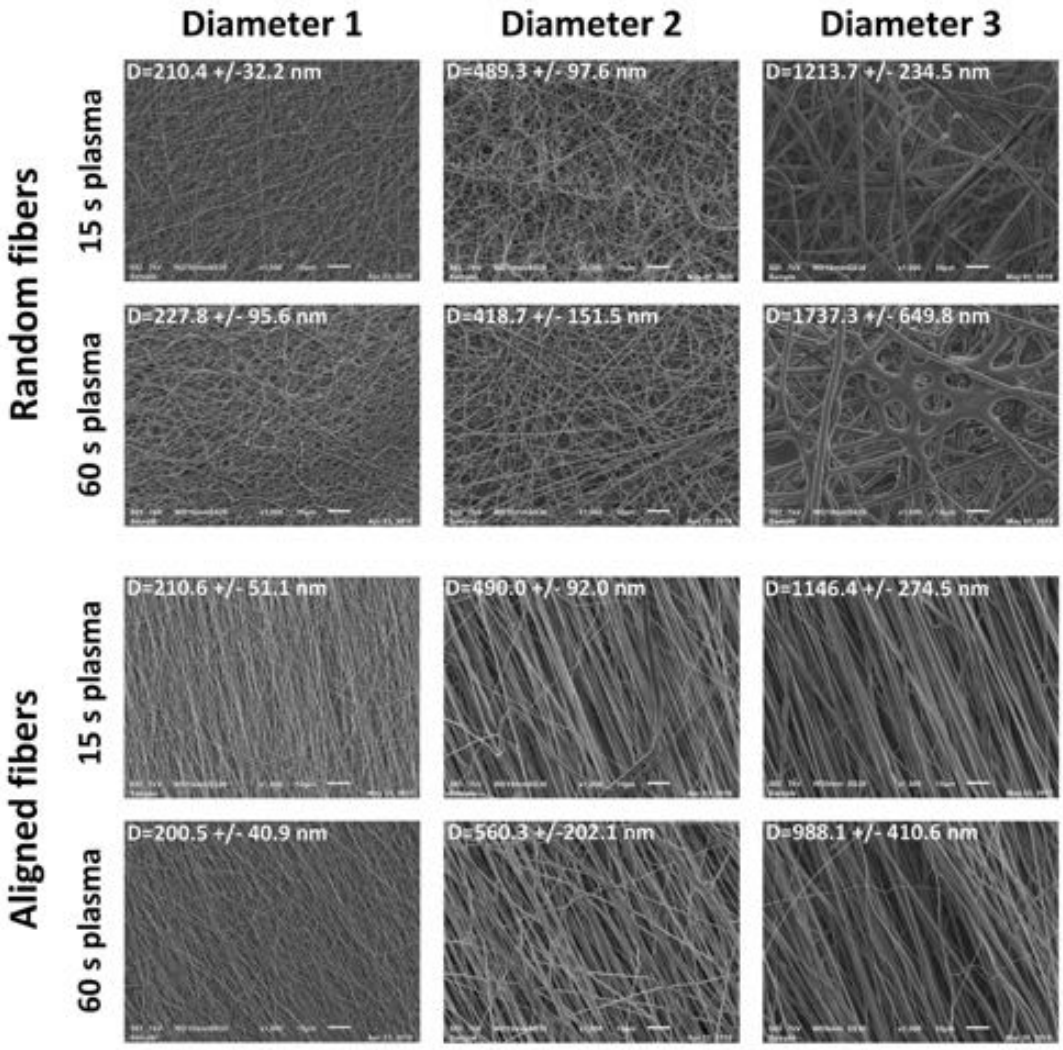

Fig. 6. SEM images of random and aligned PCL fibers subjected to argon plasma treatment of 15 s and 60 s.

4) <u>Ageing effect of plasma-treated fibers</u>

After plasma treatment, the surface has a propensity to retrogress towards its untreated hydrophobic state over time [58]. In order to have control over this unfavorable phenomenon, so-called ageing effect, PCL fibers subjected to a 15 s plasma treatment are kept in ambient air at room temperature for 1, 3 and 7 days. The possible relapse of their surface chemistry is assessed by performing XPS measurements (Fig. 7). These results reveal that the surface oxygen content slightly decreases over time with remarkably different decline profiles for the different fiber diameters and orientations. For instance, a small decrease in oxygen percentage (approximately

1%) is detected on A1 fibers 7 days post-treatment, whereas a more considerable drop (approximately 4%) is perceived on R3 fibers 7 days post-treatment. Overall, the obtained results clearly show that aligned fibers tend to withstand ageing more than random fibers. Moreover, a similar trend is observed with decreasing fiber diameters as less pronounced ageing behaviors are sensed on thinner fibers. An elucidation of the reasons underlying the ageing effect is essential for the subsequent in-deep understanding of the distinct behavior experienced by each fiber topography. Two previously described phenomena are envisaged to come into play. Firstly, the implanted polar groups have a tendency to re-orientate towards the fibers bulk in order to accommodate energetically more stable positions[31, 64]. The distinct molecular chain arrangement of the different fiber conditions is presumably intervening again in the practicability of chain movements inside the fibers and thus the ageing effect. The chains alignment and densely fastened conformation in aligned and thinner fibers hinders the movement and re-orientation of the incorporated functional groups towards the fiber bulk. In contrast, the randomness and the decreased packing density of molecular chains forming random and thicker fibers enables the plasma-induced polar groups to rotate and translate more easily. The second reason mediating the ageing behavior is the occurrence of post-plasma treatment reactions between the atmospheric surrounding minorities (e.g. CO_2 and H_2O) and the fiber surface neutralizing the inserted chemical groups [32, 58]. However, given the structure of fibrous networks, the treated fibers are not widely exposed to ambient air as neighboring fibers are shielding and protecting each other. The minor influence of post-plasma reactions can be confirmed by the negligible ageing of thin fibers undergoing a limited reorientation of their incorporated polar groups. In fact, previous results have shown that plasma-treated PCL fibers are less prone to age than PCL films as they are more exposed to air and composed of unpacked molecular chains [31-32]. It is also worth mentioning that the oxygen content on all aged fibers remains considerably higher than on the corresponding untreated samples until at least 7 days post-treatment. Nonetheless, in order to minimize the ageing effect, plasma-treated samples are sterilized and seeded with cells directly after plasma treatment.

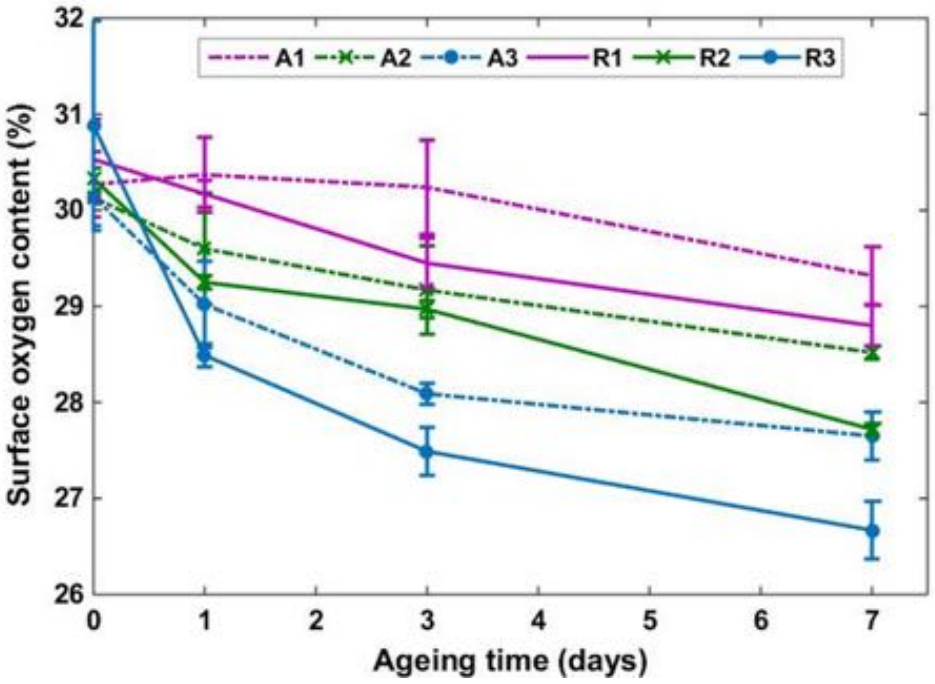

Fig. 7. Evolution of the surface oxygen percentage of PCL fibers as a function of ageing time (days) after plasma treatment.

5) In vitro cell tests

After assessing the physico-chemical properties of PCL fibers, the behavior of ADSCs grown on the different fibers are investigated in this section. The coordinated effects of the fiber size, orientation and surface chemistry on the bioresponsive processes are profoundly studied. MTT assay (day 1, 3 and 7), live-dead staining (day 1 and 7), actin staining (day 3) and SEM imaging (day 1 and 7) are performed to evaluate the cell adhesion, proliferation, viability, cytoplasmic remodeling, morphology, orientation and infiltration. The cell alignment and nucleus circularity are quantified using the actin and DAPI stained images (day 3).

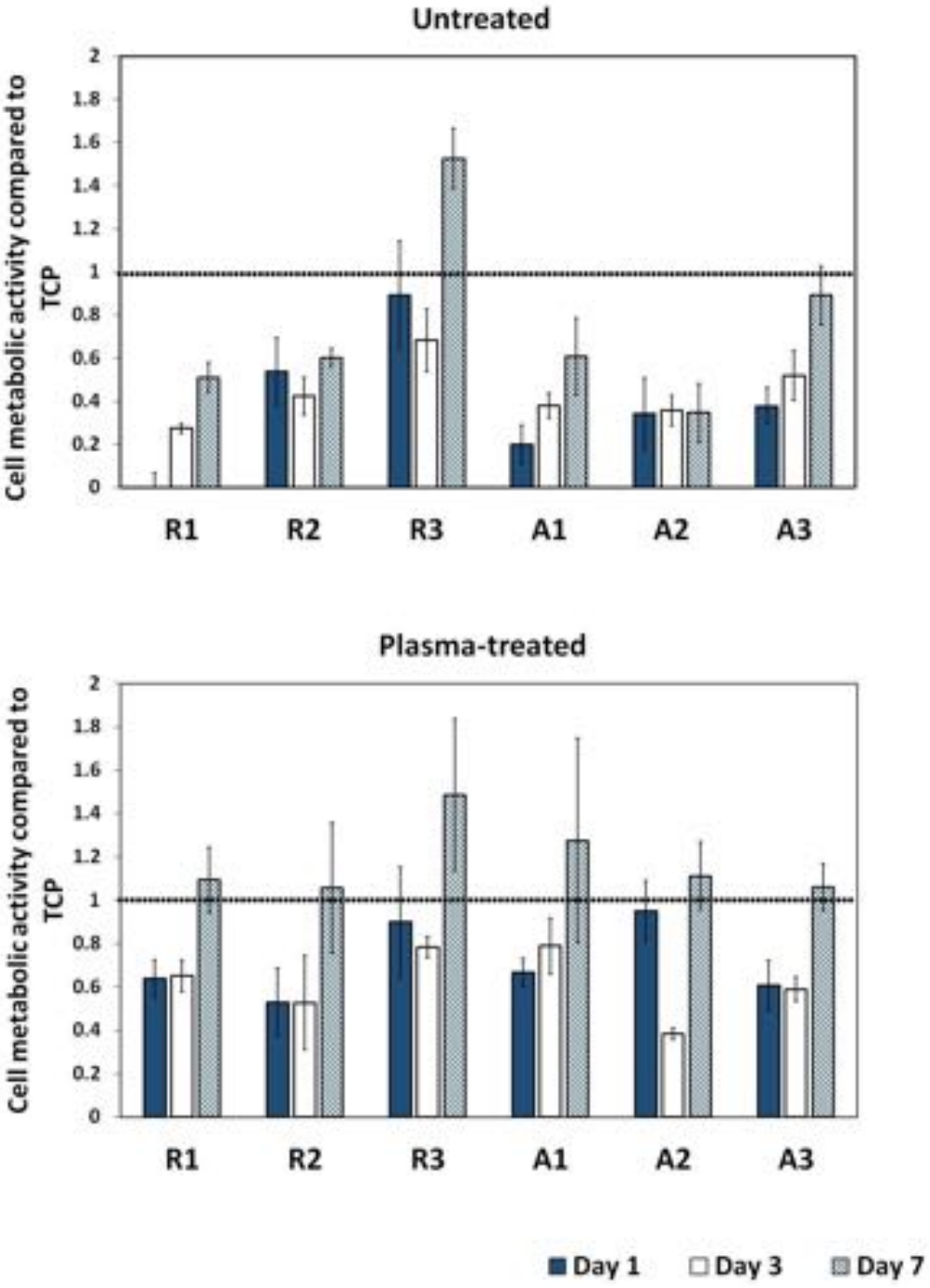

Fig. 8. Ratio of metabolically active ADSCs cultured for 1, 3 and 7 days on PCL fibers, relative to the TCP value (dotted line)

- **ADSCs on untreated fibers of different diameters:** As a first step of this multifurcate cell study, one can already notice differences in cellular performances between untreated fibers of different sizes. This is quantitatively illustrated by MTT results (Fig. 8) showing that the number of

metabolically active cells adhering (day 1) and proliferating (day 3 and 7) on the substrates increases with increasing diameter of random fibers. This trend is also present, but less distinguishable in case of aligned PCL fibers. These MTT results are in close correlation with the cellular morphology and cytoskeleton shape, as shown in Fig. 9, 10 and 11. The quantitative gradual increase in cell attachment and proliferation on increasing fiber diameters is associated with gradual enlargement and spreading of the cytoplasm and regression of cell cluster occurrence. When surface properties are biologically inappropriate, cells tend to escape the surface by forming bunches and they prefer to attach to each other rather than on the substrate, as clearly discernable on the actin staining images of the thinnest fibers (Fig. 9). In contrast, less cell clusters and some elongated cells can be detected on the thickest fibers. Nevertheless, it is worth mentioning that in case of untreated fibers, ADSCs performance remains defective even on the thickest fibers as poorly spread and rounded cells are still observed 7 days after cell seeding. The diverse cellular responses on different fiber conditions is presumably associated with the primary cell capture efficiency and cells/fibers contact in which cellular receptors, mainly the integrin proteins, play a primordial role [9, 32, 65]. The distinctive size of focal adhesion contacts of different cell types is presumably associated with their preference to specific topographical sizes [1]. Many studies have reported, in contrast to what is observed in this work, that the adhesion and subsequent proliferation of some cell types such as Schwann cells, neural stem cells, fibroblasts and osteoblasts are enhanced when decreasing the fiber size [2, 9, 15]. This finding was linked to the fact that smaller fibers have larger surface-to-volume ratio and would probably bind more cell receptors. However, ADSCs seem to have relatively wide focal adhesion complexes in comparison to small-sized nanofibers. This gives rise to fewer anchor points weakening the complexes and leading to poor cell attachment on smaller fibers. When increasing the fiber diameter, an improved recruitment of integrins takes place directing the occurrence of more anchor points and resulting in more stable focal adhesion sites [17]. This can explain the superior cell adhesion, and spreading of ADSCs on larger fibers. The same trend was also previously detected when keratinocytes were seeded on different fiber sizes as they stayed spherical on the thinnest fibers and spread out on the thickest fibers [1]. Other important characteristics affecting cell adhesion are surface chemistry, wettability and roughness. A similar surface chemistry is detected on all untreated fibers causing super-hydrophobicity characteristics which negatively influence cell attachment. Therefore, one may think that the increased roughness on larger diameters is partly affecting and improving cell

affinity. This preliminary conclusion is further confirmed by the study of Ahn et al. showing that ADSCs that were seeded on roughness gradients of polyethylene films adhered better on rougher surfaces [56]. Nonetheless, a conspicuous observation that cannot be overlooked is the stagnation of the cells metabolic activity on the intermediate fiber diameter until day 7 and on the thickest diameter until day 3 only, which indicates relatively weak cellular processes after initial adhesion (Fig. 8). This initial cell attachment is followed by a lag-stage phase during which the cells try to adapt to their surroundings. Cells that stay alive and that retain their activity during this post-adhesion phase manage to proliferate [31]. Therefore, ADSCs that attach to intermediate and thick fibers seem to be disturbed during this adaptation phase. This can be presumably attributed to the fibers depth or pattern height that were found, independently of the surface roughness, to be among the topographical factors influencing the long-term adhesion and the maturation of focal adhesions during the lag-stage [12]. The increased height of intermediate and thick fibers is thus slowing down the cell adaptation phase which causes a subsequent poor cell proliferation. Some studies have indeed reported boosted long-term cell adhesion and proliferation on lower height patterns [12-13]. The metabolic activity of cells grown on the thickest fibers, contrarily to the intermediate fibers, again markedly increased at day 7. This can be due to the slightly lower cell sensitivity to fiber height on large fibers as SEM images (Fig. 10-11) show that each cell tends to attach and elongate on a single fiber. Conversely, in case of the intermediate fiber diameter, each cell is adhering on multiple fibers, thus sensing more the fibers depth which retards its proliferation. Lastly, very few dead cells (red cells) are detected on live-dead staining images obtained 1 day after cell seeding and even fewer are seen 7 days after seeding which indicates the non-toxicity of untreated PCL nanofibers maintaining cell viability independent of their size and orientation (Fig. 12-13).

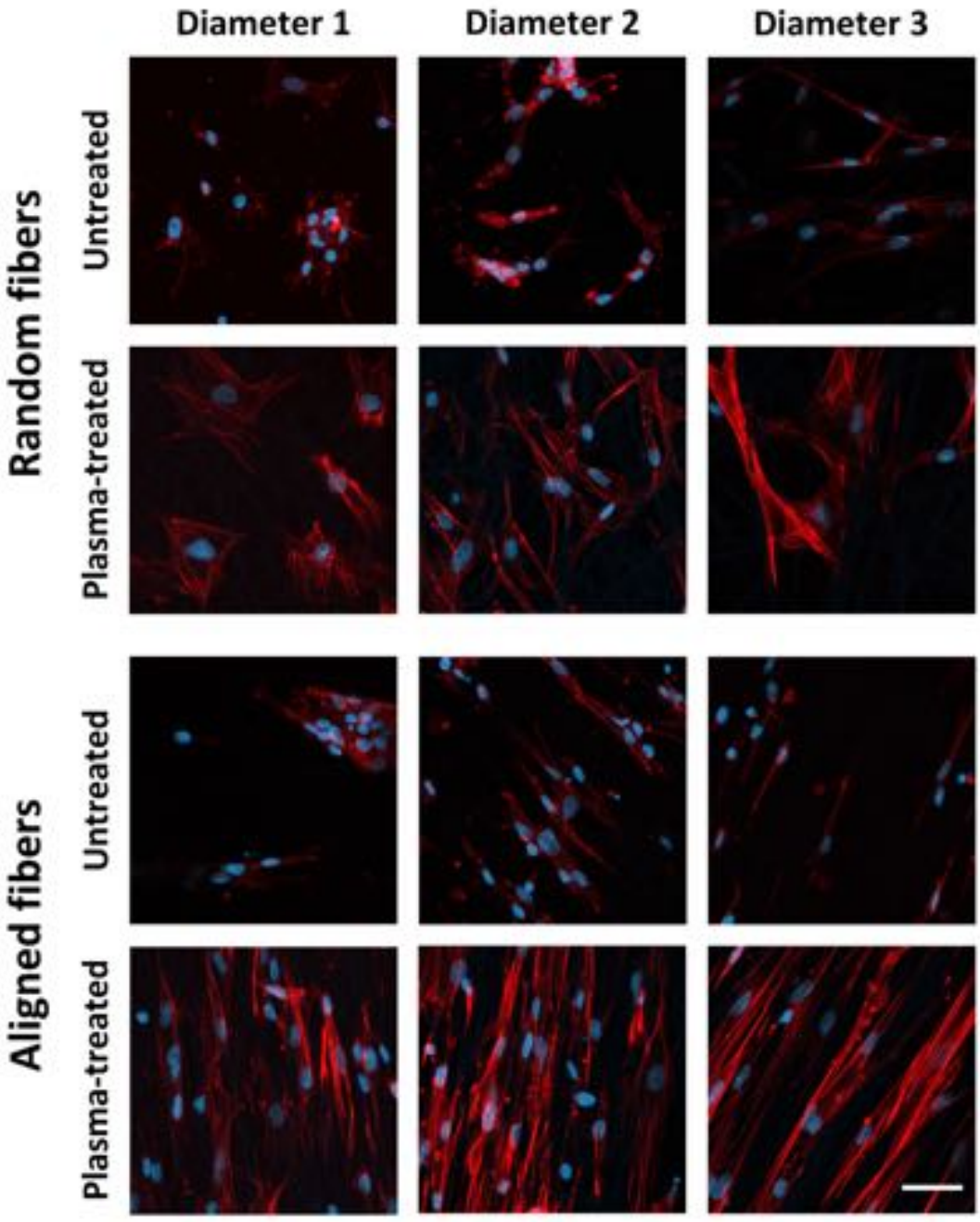

Fig. 9. Fluorescent micrographs after actin (phalloidin-rhodamin, red) and nuclei (DAPI, blue) staining of ADSCs cultured for 3 days on PCL fibers (Scale bar = 50 µm)

- **ADSCs on untreated fibers of different orientations:** Beside the fiber size, cell test results evidently reveal the great influence of fiber orientation on ADSC adhesion, proliferation and

particularly cytoskeletal reshape and morphology. First, MTT results point out a generally higher number of metabolically active cells adhering and proliferating on random fibers compared to aligned fibers at day 1, 3 and 7 of cell culturing (Fig. 8). Jahani et al. also found out an enhanced proliferation of mesenchymal stem cells on random PCL fibers compared to aligned fibers [66]. A possible explanation for this finding is the presence of more interconnected pores and multidirectional overlapping fibers forming numerous joining points on randomly deposited sheets. This random structure assists the formation of more focal adhesion complexes leading to a greater number of cells. Moreover, crossing multiple directions requires more cellular energy and thus an increased metabolic activity of ADSCs [66-67]. Deviating from the previously mentioned trend, the metabolic activity on the thinnest fibers does not differ between random and aligned fibers. This is presumably due to the fact that the probability of encountering misalignments in aligned fibers is higher for smaller fiber diameters because of the increased whipping motion that is partly in charge of thinning the fibers during electrospinning [17]. Consequently, joining fiber contacts occur more frequently on the thinnest aligned fibers leading to a cellular response similar to the one perceived on random fibers. When taking a closer look to the cell morphology, one can already notice differences between aligned and random fibers despite the cell spherical shaping and clustering tendency on untreated samples (Fig. 10-11). Actin staining and especially live-dead staining illustrate that the cells starting to spread out are aligned in the main axis direction of the aligned fibers while they are randomly oriented on random fibers (Fig. 9, 12, 13). These observations emphasize the great potential of fiber alignment in providing cell contact guidance. Some other cell types such as neural stem cells, fibroblasts, embryonic stem cells and mesenchymal stem cells were also shown to elongate along the main axis of aligned fibers and to spread arbitrarily on random fibers [17-18, 66-67]. This is due to the alignment of focal complexes on aligned fibers during the focal adhesion phase described earlier. Moreover, a traction force is exerted on the actin cytoskeleton in the same direction of aligned fibers promoting protrusions and actin polymerization parallel to the underlying fibers. This reveals again the extremely precise interplay between the substrate and the cytoskeleton filaments, particularly the actin filaments as actin disrupting agents previously attenuated cellular alignment [2]. Live-dead staining results do not reveal any differences in cell viability between random and aligned fibers (Fig. 12-13).

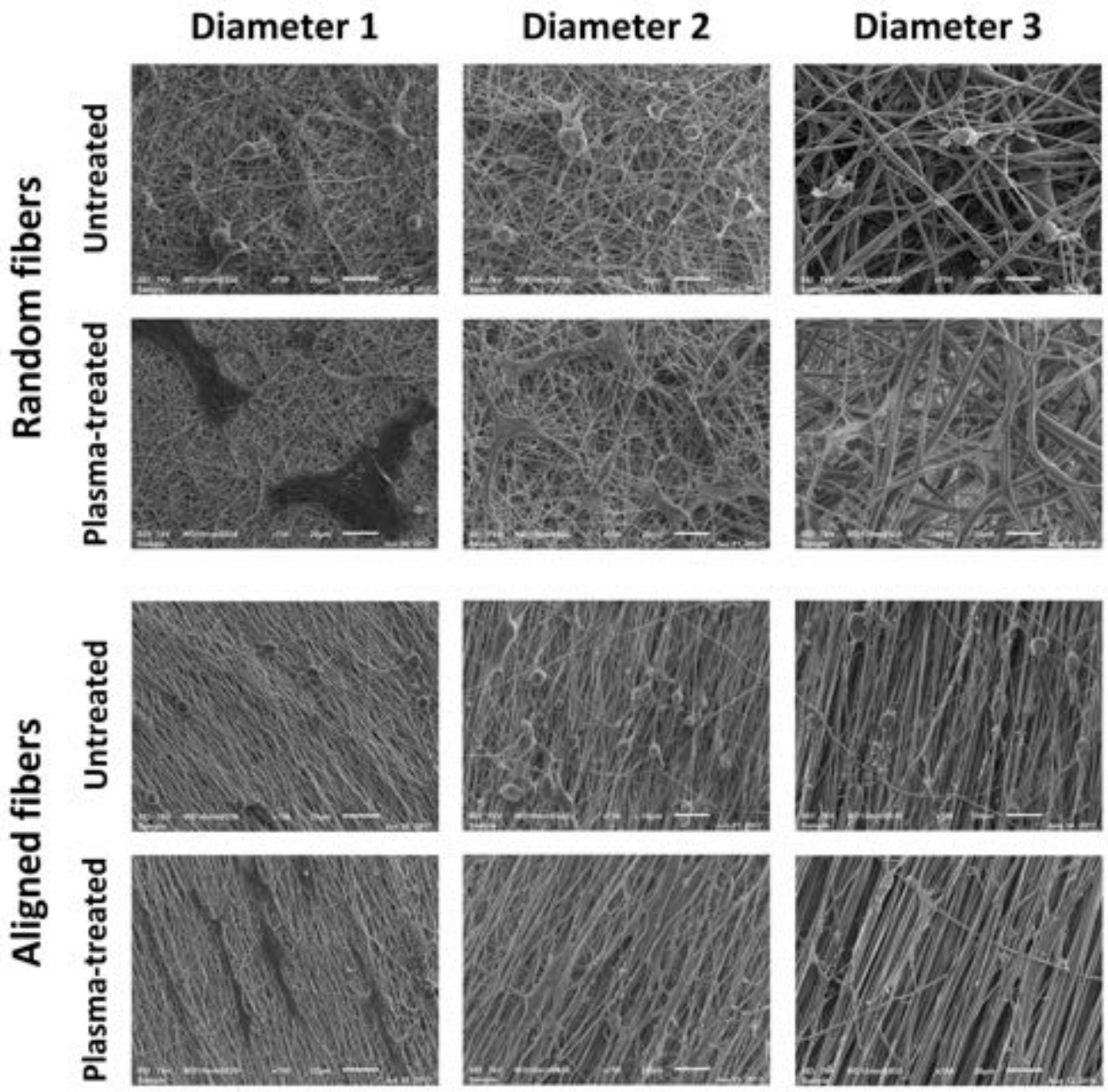

Fig. 10. SEM images of ADSCs cultured for 1 day on PCL fibers of different conditions (Scale bar = 20 μm)

- **ADSCs on untreated versus plasma-treated fibers:** Plasma treatment strikingly transfigures ADSCs bio-response to PCL nanofibers of all topographical conditions. First, a significant increase in the number of metabolically active ADSCs is detected on the plasma-treated fibers with

the smallest and intermediate diameters compared to their untreated counterparts (Fig. 8). However, the number of viable cells adhering (day 1) and proliferating (days 3-7) on the thickest fibers does not significantly differ between untreated and plasma-treated samples, given that adhesion and proliferation were already improved when increasing fiber diameter (Fig. 8). Chaurey et al. also detected a greater enhancement of fibroblast adhesion on small fibers compared to thick fibers after surface functionalization by poly-L-lysine [17]. Although plasma functionalization does not exhibit large cell density differences on all fiber conditions, great differences in ADSCs morphology can however be detected even on the thickest fiber diameters. Actin staining images (Fig. 9) clearly show the disappearance of cell clusters on treated fibers, which is the first sign of enhanced cell attachment to the surface. Moreover, cell shape and dispersion change markedly, as very well spread out and dispersed cells covering almost the entire surface are visualized: star-like and spindle-shaped cells are mainly detected on random fibers, while well-elongated and parallel cells are spotted on aligned fibers (Fig. 9). More evident distinctions are noticed on the SEM images that show, regardless of the fiber condition, completely rounded 3D cells with tiny cell areas in close contact with untreated fibers and 2D planar and stretched out cells firmly fastened to plasma-treated fibers (Fig. 10-11). Additionally, cells on the plasma-treated samples tend to infiltrate in the fibrous mesh especially in case of the thickest fibers. This enhanced ADSCs performance is attributed to the increased plasma-induced hydrophilicity that allows for the adsorption of more proteins without altering their natural conformation. Consequently, more cellular receptors can bind to the adsorbed proteins leading to numerous focal adhesive sites enhancing cell adhesion. Contrarily, the super-hydrophobicity of untreated fibers severely hampers protein adsorption and therefore limits the focal adhesion resulting in barely attached ball-shaped cells[31-32, 48]. In-deep analysis elucidates that the introduced oxygen-containing functionalities responsible for the increased wettability are specifically correlated with the enhanced cell adherence and growth. Carboxyl, carbonyl and hydroxyl groups, that steadily bind proteins, recruit more integrins and act as a glue strongly connecting and stabilizing the anchor points of focal adhesive complexes [28, 42, 65]. Therefore, the few anchor points that might still arise on smaller fibers, as described previously, are strengthened which explains the markedly improved adhesion and subsequent proliferation. Moreover, it is known that tensile forces are generated by the cells to resist the fibers and that an isometric tension is boosted within the cell when its receptors bind to proteins. These forces alter the remodeling of cytoskeletal filaments causing their

reassembly and changing the cell morphology from 2D to 3D after initial adhesion [65]. This can explain the long-standing 3D cell rounded shape on untreated fibers even after 7 days of cell culturing. Nevertheless, the stable focal adhesion sites induced by the oxygen-containing groups are probably hindering the cytoskeletal reassembly in case of plasma-treated fibers, which justifies the irreversible 2D planar shape of cells after their adhesion. Prabhakaran et al. underlined the particular importance of plasma-induced surface oxygen groups by obtaining an improved Schwann cell adhesion on air plasma-treated PCL fibers, not only in comparison to untreated fibers, but also when comparing to PCL/collagen fibers [68]. Other studies also showed that the cytocompatibility of other cell types such as osteoblasts, embryonic stem cells, endothelial cells and chondrocytes is significantly boosted on plasma-treated PCL fibers [21, 28, 42, 67]. Lastly, plasma treatment does not seem to have a toxic effect on the cells as almost no dead ADSCs are detected on the live-dead staining images of day 1 and very few dead cells are perceived at day 7 (Fig. 12-13). As plasma treatment is favoring cellular infiltration in-between the fibers, the presence of dead cells at day 7 might be due to the PBS inability to rinse away the infiltrated cells that did not survive during the lag-stage.

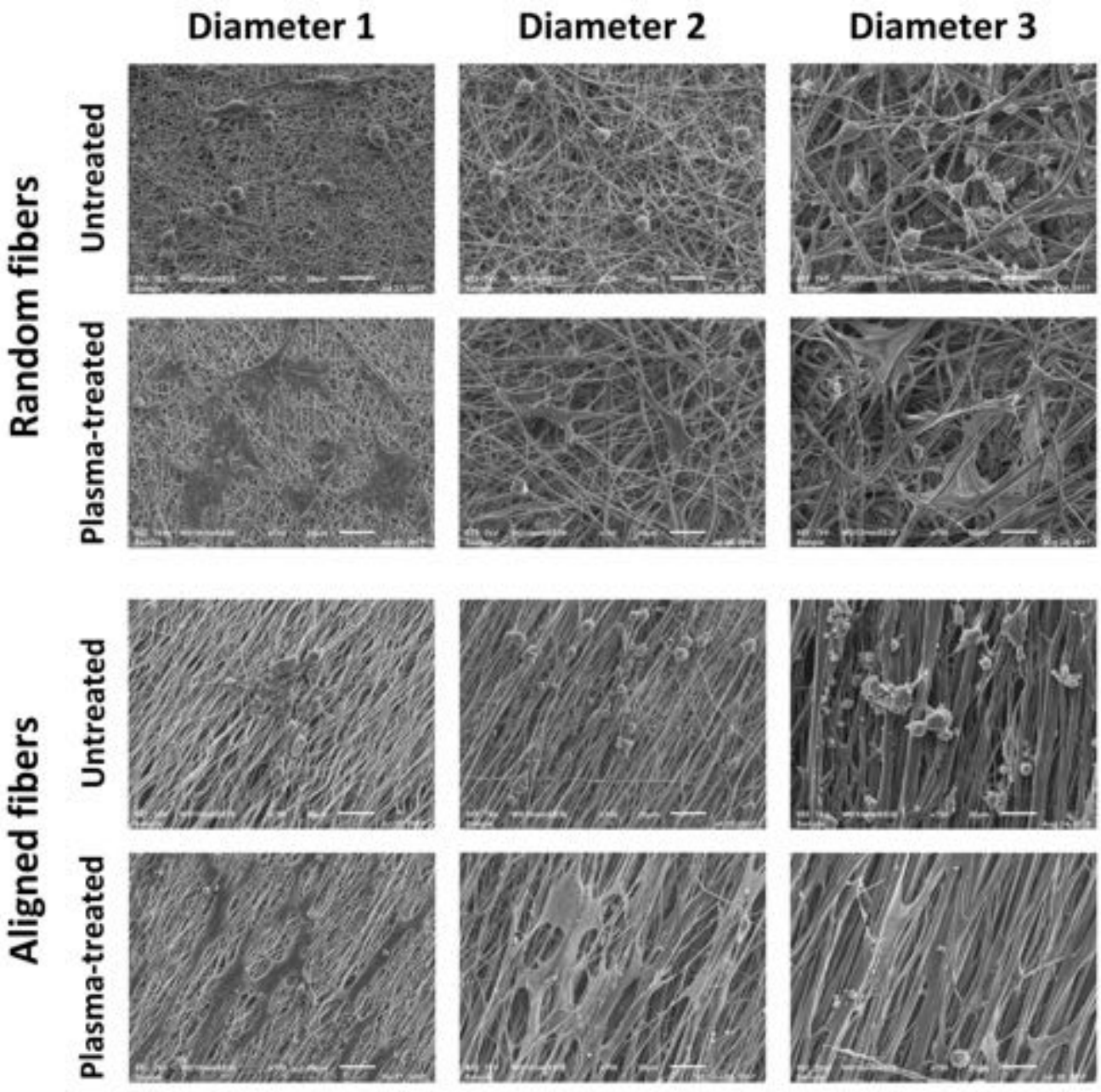

Fig. 11. SEM images of ADSCs cultured for 7 days on PCL fibers of different conditions (Scale bar = 20 μm)

- **ADSCs on plasma-treated fibers of different diameters:** When taking a closer look at the plasma-treated fibers of different diameters, one can notice some variations in ADSCs behavior. As already mentioned, MTT results show a bigger post-treatment enhancement of cell density at day 1, 3 and 7 on the thinnest fibers as these fibers had the poorest cytocompatibility prior to the

plasma treatment (Fig. 8). This observation can be linked to the different surface wettability between the thinnest fibers on the one hand and the intermediate and thickest fibers on the other hand. After plasma treatment, A1 and R1 saturate at a WCA of 19° and 25° respectively, while larger fibers were fully penetrated by water, their WCA being 0°. Despite the positive effect of hydrophilicity in enhancing protein adsorption, the super-hydrophilicity of thick fibers seems to be a limiting factor. Protein adsorption takes place when proteins displace the water molecules adsorbed on the surface. This displacement becomes difficult on super-hydrophilic surfaces as they exhibit a greater electrostatic force at the water/solid interface [48]. This explains the minor ADSCs density improvement on thick fibers. In fact, previous studies have shown that each cell type favors a particular surface wettability. For instance, fibroblasts and endothelial cells adhere better on surfaces with a WCA of 55° while osteoblasts prefers a WCA of 64° [5, 32]. ADSCs were also noticed to behave better on polymer films with moderate hydrophilicity (≈ 60°) [31, 56]. Controlling the WCA of the PCL fibers to attain a moderate hydrophilicity while introducing a maximal amount of oxygen-containing groups is very difficult, if not impossible. Nonetheless, the increased surface area and roughness of the fibers compared to films comes to compensate the excessive fiber hydrophilicity as ADSCs were perceived to adhere better on rough surfaces.

Similar to what is observed for the untreated fibers, a stagnation or even decrease in cell metabolic activity is distinguished on plasma-treated fibers at day 3. This observation can be attributed to the depth of the intermediate and thicker fibers negatively affecting the ADSCs during the lag-stage. However, in contrast to the untreated fibers, a remarkable increase in ADSCs metabolic activity is again seen at day 7 especially in case of the intermediate fibers, indicative of outstanding proliferation (Fig. 8). Pappa et al. also obtained, based on MTT results of fibroblasts grown on plasma-treated PCL fibers, a decrease in metabolic activity at day 3 and subsequent increase at day 7 [33].

Actin staining and SEM images (Fig. 9-11) of plasma-treated random fibers visualize a gradual change from dilated and more circular cell shape to stretched out and more elongated cell shape on fibers with increasing diameters. ADSCs adhere on multiple fibers and therefore extend multi-directionally on the smallest fibers. A different trend is observed for thicker fibers: cells continue to adhere on multiple fibers but extend along a few preferred fiber axes on R2 and along one preferred fiber axis on R3. Given the fact that the length of an R3 fiber in between crosslinks is relatively large compared to the ADSC dimension, a partial alignment of the cells is sensed. At

some points where numerous fibers converge, ADSCs still stretch multi-directionally. These ADSCs morphologies are consistent with other cell types such as neural stem cells and Schwann cells when seeded on random fibers of different sizes [9, 69]. An ADSC bipolar and parallel fashion is however observed on aligned fibers compared to the multipolar cell shape on random fibers. When increasing the fiber size, each cell tends to attach to fewer number of fibers to a point where one cell is not anymore distinguished from a fiber on the thickest diameters.

A distinction of the essence, clearly observed on the SEM images (Fig. 10-11), is the infiltration of ADSCs in between the pores of plasma-treated R3 fibers, and to a lower extend of R2 fibers mainly at day 7. The synchronic effect of larger pore size and plasma-optimized surface chemistry resulted into this deep and complete cell colonization of the fibrous mesh.

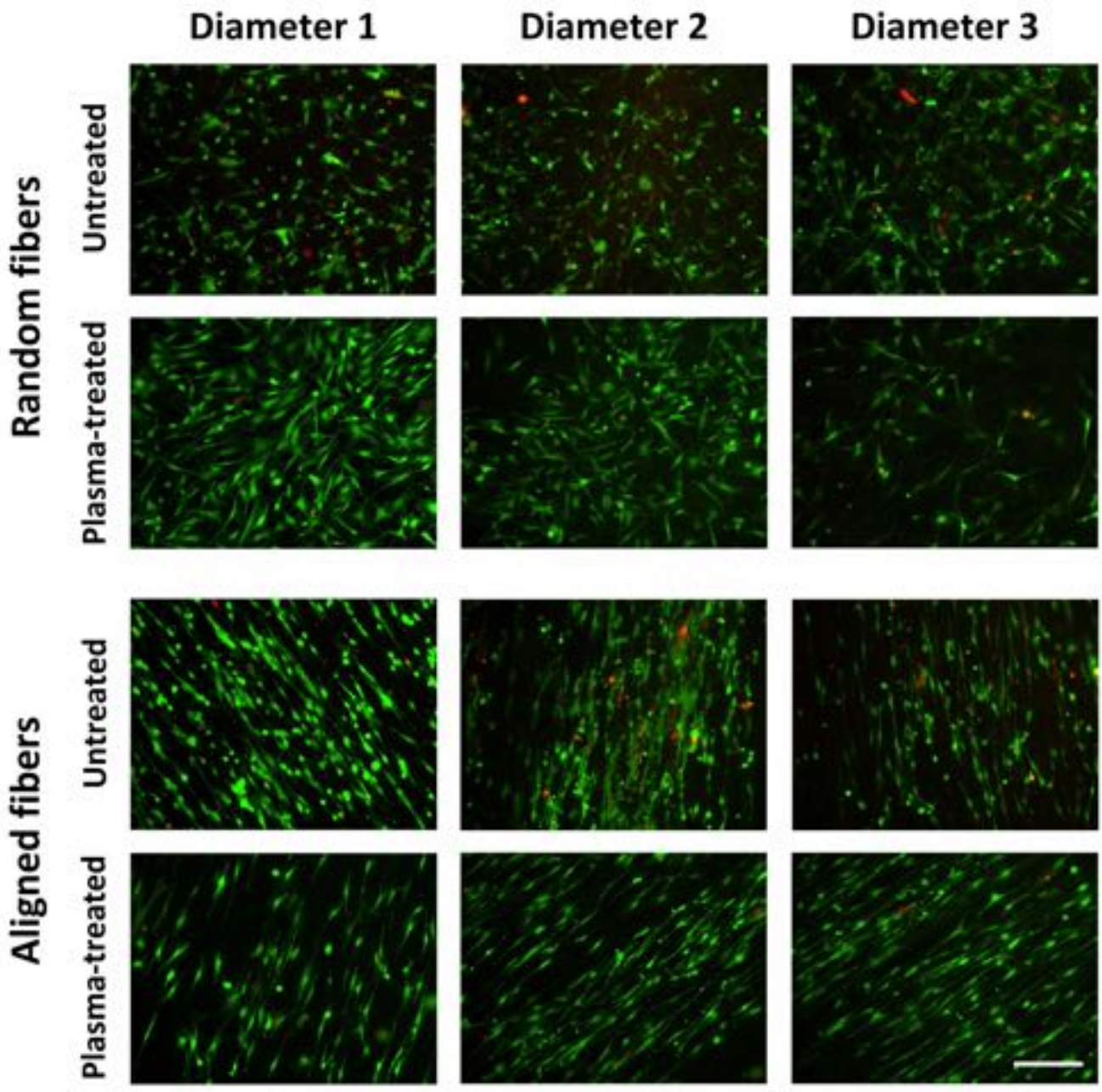

Fig. 12. Fluorescent images after live/dead staining of ADSCs cultured for 1 day on PCL fibers of different conditions (Scale bar = 200 μm)

- ADSCs on plasma-treated fibers of different orientations: After subjecting the aligned fibers to a plasma treatment, significant differences in ADSCs metabolic activity are no longer perceived compared to random fibers (Fig. 8). The presence of less fibrous joining points that reduces the amount of focal adhesion complexes on aligned fibers, is compensated by the incorporated polar

groups strengthening these fewer adhesion sites. Therefore, similar adhesion efficiency and subsequent proliferation are detected on both fiber orientations. A more discernable difference in cell morphology is however visualized between aligned and random fibers after plasma treatment. In addition to live-dead staining images (Fig. 12-13), SEM images also show the enhanced and complete alignment of ADSCs on aligned fibers and the absence of rounded cells (Fig. 10-11). Actin staining images come to corroborate these observations by highlighting the bi-directionally overextended cytoplasm of ADSCs on aligned fibers (Fig. 9). In fact, a quantitative confirmation of this finding can be concluded from the pixel intensity histograms of the FTT output images plotted in function of the acquisition angle of the cells (Fig. 14-A). The overall data point distribution shows higher and narrower peaks on the aligned fibers of different diameters in comparison to their random counterpart. This indicates that the cells are more accurately aligned on the aligned fibers with respect to the specific orientation axis of the underlying fibers. The low and wide distribution curve of random fibers reveals the arbitrary shape of cells grown on the multiple orientation axes of random fibers. An important distinction is the improved cell alignment on the biggest diameter of the aligned fibers proven by the further upgraded height and narrowness of the distribution curve. This can be explained by the increased probability of encountering misalignments on smaller fibers which deviates the cell that can continue growing in another direction. Moreover, each cell tends to attach to only one fiber of the biggest diameter leading to its overextension in the direction adopted by the neighboring cells growing on parallel fibers. The cell bipolar elongation can narrow the cytoplasm extensively to a point where the nuclei become compressed and therefore adopt a polygonal shape instead of a circular shape. This is visually discernable on the actin staining images of the plasma-treated aligned fibers. The nucleus circularity values on the different fiber conditions represent a quantitative affirmation of this observation (Fig.14-B). The cell nuclei on the untreated and plasma-treated random fibers have a circularity between 0.7 and 0.9 indicative of a more rounded shape because of the circular and multipolar cytoplasm. Rounded nuclei are still detected on untreated aligned fibers which shows the limited ability of the cell to extensively elongate. In contrast, a statistically different nucleus circularity value (around 0.5), indicative of a more elongated shape, is detected on the plasma-treated aligned fibers. This confirms again the positive effect of plasma in allowing a robust attachment and elongation of the cells that overextend to a point where their nuclei elongate as well.

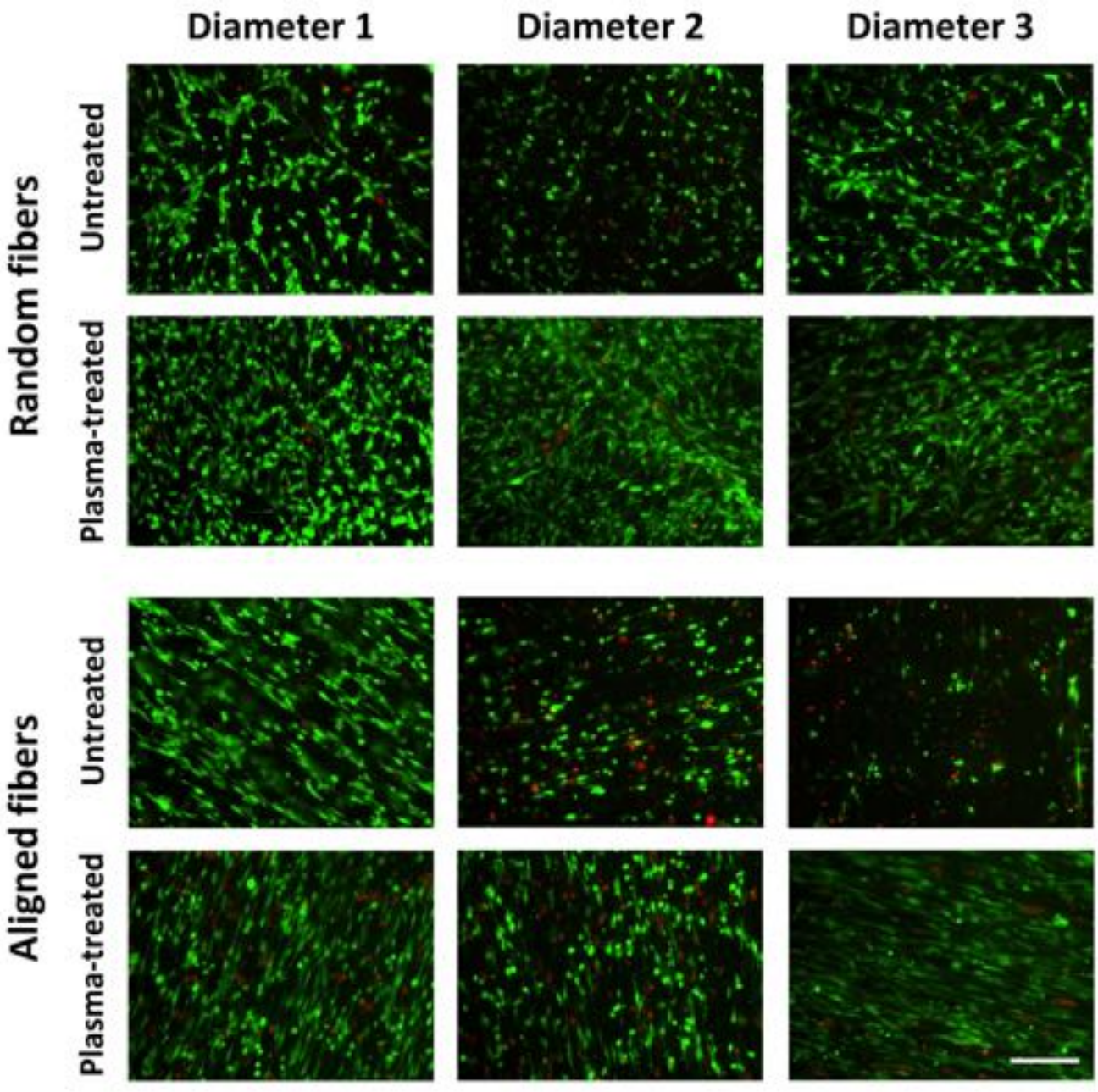

Fig. 13. Fluorescent images after live/dead staining of ADSCs cultured for 7 days on PCL fibers of different conditions (Scale bar = 200 μm)

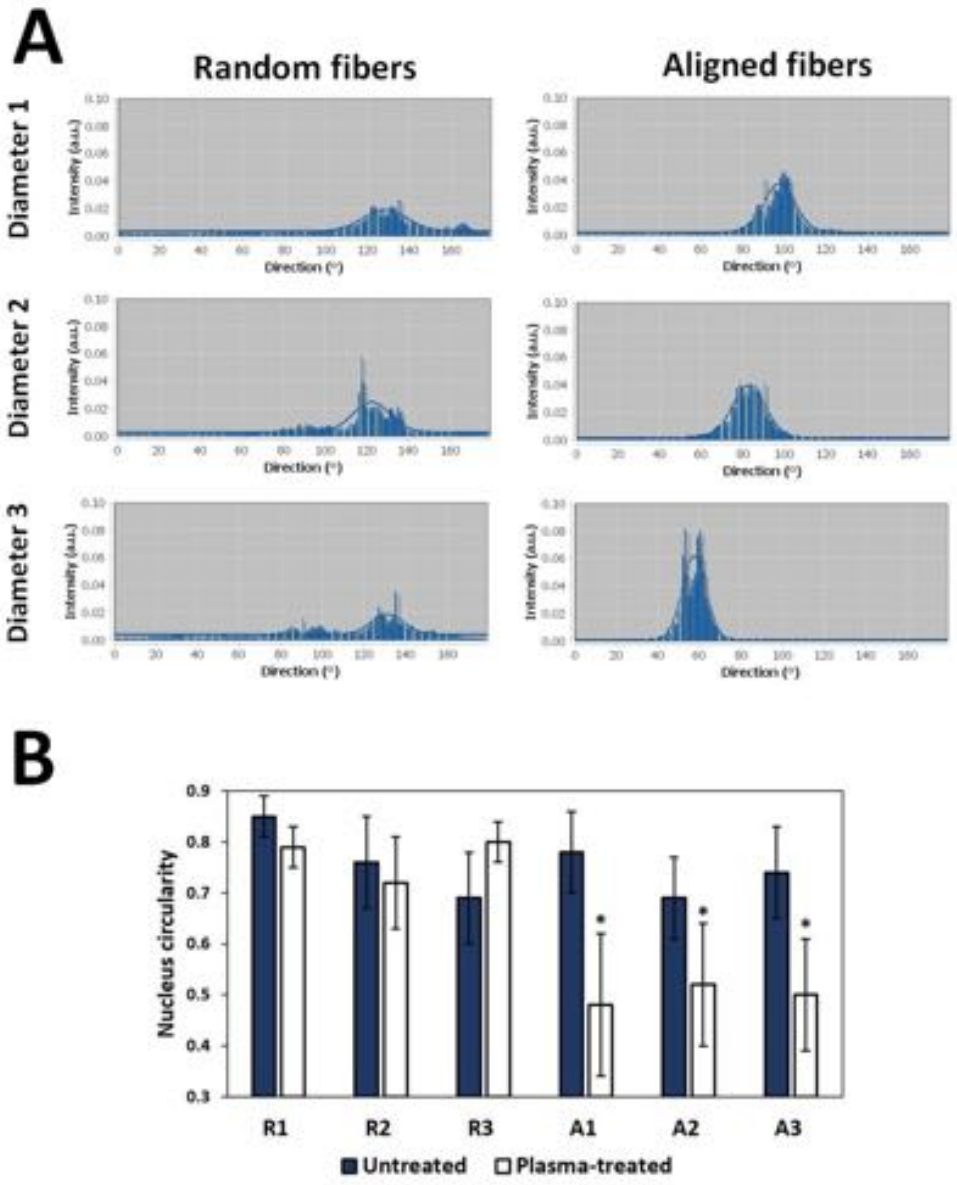

Fig.14. FTT pixel intensity plots in function of the direction of the cells grown on plasma-treated fibers (A) and nucleus circularity of the cells grown on all fiber conditions (B) (*: statistically significant difference with respect to untreated fibers and random fibers)

IV- Conclusion

This present study highlights the synergistic effect of PCL fiber size, orientation and surface chemistry on the performance of adipose-derived stem cells. First, random and aligned fibers of 3 different diameters each are subjected to a DBD plasma treatment operating in argon at medium pressure, after which their physico-chemical properties are deeply examined pre- and post-

treatment. XPS and WCA results reveal the prominent efficiency of plasma in enhancing the fibers hydrophilicity by grafting oxygen-containing polar groups on their surface. Despite the incorporation of approximately the same oxygen amount on all samples, WCA values significantly differ between the different fiber sizes and orientations thus emphasizing the outstanding influence of the fibrous mesh topography on the liquid-solid interface. SEM analysis shows that argon treatment, in contrast to previously studied air DBD treatments, preserves the fiber morphology and scale after 15 s of plasma exposure which corresponds to the surface chemical saturation. Nevertheless, newly designed DBDs with advanced configurations involving for instance curved electrodes were shown to prevent nanofiber etching and degradation when operating in air. An extended plasma exposure of 1 min starts altering the fibers morphological features with a growing risk of drastic damaging on thicker and random fibers compared to thinner and aligned fibers. The diverse responses to plasma stem from the distinct molecular chain arrangement and crystallinity of different fiber diameters and orientations. After analyzing the surface properties of untreated and plasma-treated fibers, ADSCs are also seeded on all samples under study. The bioresponsive processes arising from the interaction of the cell cytoskeleton and the fibers are profoundly examined based on the strongly coordinated interplay between fiber size, orientation and surface chemistry effects. Some distinctions in cell performance can already be distinguished on the untreated fibers of different diameters. A gradual increase in cell density and cytoplasm spreading is observed with increasing fiber diameter. This is presumably due to the wide focal adhesion complexes of ADSCs giving rise to fewer anchor points on small fibers leading to poor cell attachment and subsequent proliferation. Generally, the improved surface chemistry of plasma-treated fibers strikingly enhances the cell metabolic activity, adhesion, proliferation, cytoplasmic remodeling and morphology on all topographical conditions. ADSCs adhere on random fibers in a multi-directional fashion with a gradual change from dilated and more circular to stretched out and more elongated morphology on increasing diameters. In contrast, cells overextend and align in parallel and bi-polar fashion on aligned fibers with a tendency to attach on fewer fibers when increasing their size. An important distinction is the infiltration of cells in-between the pores of the thickest and plasma-treated fibers. Overall, non-thermal plasma technology constitutes a very promising surface treatment for successful fibrous implants of multiple tissue engineering applications. As the desired ADSCs performance strongly depends on a specific end-application, appropriate fiber size and orientation can thus be selected accordingly. Therefore, this paper

represents an on-target reference paving the way towards the optimization of the previous generation of biomaterials.

V- Acknowledgments

The research leading to these results has received funding from the European Research Council under the European Union's Seventh Framework Program [FP/2007-2013]: ERC Grant Agreement number 335929 [PLASMATS]. All authors also acknowledge the support of the Special Research Fund [BOF 14/IOP/045] of Ghent University. Pieter Cools specifically would also like to thank the Special Research Fund of Ghent University for financing his post-doctoral grant.

VI- References

1. Pelipenko, J.; Kocbek, P.; Kristl, J., Nanofiber diameter as a critical parameter affecting skin cell response. *Eur. J. Pharm. Sci.* **2015,** *66*, 29-35.
2. Kim, D.-H.; Provenzano, P. P.; Smith, C. L.; Levchenko, A., Matrix nanotopography as a regulator of cell function. *J. Cell. Biol.* **2012,** *197* (3), 351-360.
3. Supaphol, P.; Suwantong, O.; Sangsanoh, P.; Srinivasan, S.; Jayakumar, R.; Nair, S. V., Electrospinning of Biocompatible Polymers and Their Potentials in Biomedical Applications. In *Biomedical Applications of Polymeric Nanofibers*, Jayakumar, R.; Nair, S., Eds. Springer Berlin Heidelberg, 2012; pp 213-239.
4. O'brien, F. J., Biomaterials & scaffolds for tissue engineering. *Mater. Today.* **2011,** *14* (3), 88-95.
5. Ghobeira, R.; De Geyter, N.; Morent, R., Plasma surface functionalization of biodegradable electrospun scaffolds for tissue engineering applications. In *Biodegradable polymers: recent developments and new perspectives*, Rohman, G., Ed. IAPC Publishing: Zagreb Croatia, 2017; pp 191-236.
6. Yim, E. K.; Leong, K. W., Significance of synthetic nanostructures in dictating cellular response. *Nanomedicine.* **2005,** *1* (1), 10-21.
7. Gupta, D.; Venugopal, J.; Prabhakaran, M. P.; Dev, V. G.; Low, S.; Choon, A. T.; Ramakrishna, S., Aligned and random nanofibrous substrate for the in vitro culture of Schwann cells for neural tissue engineering. *Acta. Biomater.* **2009,** *5* (7), 2560-2569.
8. Haider, A.; Haider, S.; Kang, I.-K., A comprehensive review summarizing the effect of electrospinning parameters and potential applications of nanofibers in biomedical and biotechnology. *Arab. J. Chem.* **2015**.
9. Gnavi, S.; Fornasari, B.; Tonda-Turo, C.; Ciardelli, G.; Zanetti, M.; Geuna, S.; Perroteau, I., The influence of electrospun fibre size on Schwann cell behaviour and axonal outgrowth. *Mater. Sci. Eng. C.* **2015,** *48*, 620-631.
10. Morent, R.; De Geyter, N.; Desmet, T.; Dubruel, P.; Leys, C., Plasma surface modification of biodegradable polymers: a review. *Plasma Process. Polym.* **2011,** *8* (3), 171-190.
11. Woodruff, M. A.; Hutmacher, D. W., The return of a forgotten polymer—Polycaprolactone in the 21st century. *Prog. Polym. Sci.* **2010,** *35* (10), 1217-1256.
12. Nguyen, A. T.; Sathe, S. R.; Yim, E. K., From nano to micro: topographical scale and its impact on cell adhesion, morphology and contact guidance. *J. Phys. Condens. Matter.* **2016,** *28* (18), 183001.

13. Jeon, H.; Simon, C. G.; Kim, G., A mini-review: cell response to microscale, nanoscale, and hierarchical patterning of surface structure. *J. Biomed. Mater. Res. B Appl. Biomater.* **2014,** *102* (7), 1580-1594.
14. Leong, K. W.; Yim, E. K., Significance of Synthetic Nanostructures in Dictating Cellular Response. In *Nanomedicine in Cancer*, Pan Stanford: 2017; pp 129-158.
15. Chen, M.; Patra, P. K.; Warner, S. B.; Bhowmick, S., Role of Fiber Diameter in Adhesion and Proliferation of NIH 3T3 Fibroblast on Electrospun Polycaprolactone Scaffolds. *Tissue Eng.* **2007,** *13* (3), 579-587.
16. Badami, A. S.; Kreke, M. R.; Thompson, M. S.; Riffle, J. S.; Goldstein, A. S., Effect of fiber diameter on spreading, proliferation, and differentiation of osteoblastic cells on electrospun poly (lactic acid) substrates. *Biomaterials.* **2006,** *27* (4), 596-606.
17. Chaurey, V.; Block, F.; Su, Y.-H.; Chiang, P.-C.; Botchwey, E.; Chou, C.-F.; Swami, N. S., Nanofiber size-dependent sensitivity of fibroblast directionality to the methodology for scaffold alignment. *Acta. Biomater.* **2012,** *8* (11), 3982-3990.
18. He, L.; Liao, S.; Quan, D.; Ma, K.; Chan, C.; Ramakrishna, S.; Lu, J., Synergistic effects of electrospun PLLA fiber dimension and pattern on neonatal mouse cerebellum C17. 2 stem cells. *Acta. Biomater.* **2010,** *6* (8), 2960-2969.
19. Chew, S. Y.; Mi, R.; Hoke, A.; Leong, K. W., The effect of the alignment of electrospun fibrous scaffolds on Schwann cell maturation. *Biomaterials* **2008,** *29* (6), 653-661.
20. Koh, H.; Yong, T.; Chan, C.; Ramakrishna, S., Enhancement of neurite outgrowth using nano-structured scaffolds coupled with laminin. *Biomaterials.* **2008,** *29* (26), 3574-3582.
21. Recek, N.; Resnik, M.; Motaln, H.; Lah-Turnšek, T.; Augustine, R.; Kalarikkal, N.; Thomas, S.; Mozetič, M., Cell adhesion on polycaprolactone modified by plasma treatment. *Int. J. Polym. Sci.* **2016,** *2016*.
22. Kleinman, H. K.; Philp, D.; Hoffman, M. P., Role of the extracellular matrix in morphogenesis. *Curr. Opin. Biotech.* **2003,** *14* (5), 526-532.
23. Swindle-Reilly, K. E.; Paranjape, C. S.; Miller, C. A., Electrospun poly (caprolactone)-elastin scaffolds for peripheral nerve regeneration. *Prog. Biomater.* **2014,** *3* (1), 20.
24. Neal, R. A.; Tholpady, S. S.; Foley, P. L.; Swami, N.; Ogle, R. C.; Botchwey, E. A., Alignment and composition of laminin–polycaprolactone nanofiber blends enhance peripheral nerve regeneration. *J. Biomed. Mater. Res. A.* **2012,** *100* (2), 406-423.
25. Cohn, C.; Leung, S.; Crosby, J.; Lafuente, B.; Zha, Z.; Teng, W.; Downs, R.; Wu, X., Lipid-mediated protein functionalization of electrospun polycaprolactone fibers. *Express Polym. Lett.* **2016,** *10* (5), 430.
26. Jin, G.; Prabhakaran, M. P.; Ramakrishna, S., Stem cell differentiation to epidermal lineages on electrospun nanofibrous substrates for skin tissue engineering. *Acta. Biomater.* **2011,** *7* (8), 3113-3122.
27. Zeugolis, D. I.; Khew, S. T.; Yew, E. S.; Ekaputra, A. K.; Tong, Y. W.; Yung, L.-Y. L.; Hutmacher, D. W.; Sheppard, C.; Raghunath, M., Electro-spinning of pure collagen nano-fibres–just an expensive way to make gelatin? *Biomaterials.* **2008,** *29* (15), 2293-2305.
28. Martins, A.; Pinho, E. D.; Faria, S.; Pashkuleva, I.; Marques, A. P.; Reis, R. L.; Neves, N. M., Surface Modification of Electrospun Polycaprolactone Nanofiber Meshes by Plasma Treatment to Enhance Biological Performance. *Small.* **2009,** *5* (10), 1195-1206.
29. Jiao, Y.-P.; Cui, F.-Z., Surface modification of polyester biomaterials for tissue engineering. *Biomed. Mater.* **2007,** *2* (4), R24.
30. Cools, P.; Mota, C.; Lorenzo-Moldero, I.; Ghobeira, R.; De Geyter, N.; Moroni, L.; Morent, R., Acrylic Acid Plasma Coated 3D Scaffolds for Cartilage tissue engineering applications. *Sci. Rep.* **2018,** *8* (1), 3830.
31. Ghobeira, R.; Philips, C.; Declercq, H.; Cools, P.; De Geyter, N.; Cornelissen, R.; Morent, R., Effects of different sterilization methods on the physico-chemical and bioresponsive properties of plasma-treated polycaprolactone films. *Biomed. Mater.* **2017,** *12* (1), 015017.

32. Ghobeira, R.; Philips, C.; De Naeyer, V.; Declercq, H.; Cools, P.; De Geyter, N.; Cornelissen, R.; Morent, R., Comparative Study of the Surface Properties and Cytocompatibility of Plasma-Treated Poly-ε-Caprolactone Nanofibers Subjected to Different Sterilization Methods. *J. Biomed. Nanotechnol.* **2017,** *13* (6), 699-716.
33. Pappa, A. M.; Karagkiozaki, V.; Krol, S.; Kassavetis, S.; Konstantinou, D.; Pitsalidis, C.; Tzounis, L.; Pliatsikas, N.; Logothetidis, S., Oxygen-plasma-modified biomimetic nanofibrous scaffolds for enhanced compatibility of cardiovascular implants. *Beilstein J. Nanotechnol.* **2015,** *6*, 254.
34. Yari, A.; Teimourian, S.; Amidi, F.; Bakhtiyari, M.; Heidari, F.; Sajedi, N.; Veijouye, S. J.; Dodel, M.; Nobakht, M., The role of biodegradable engineered random polycaprolactone nanofiber scaffolds seeded with nestin-positive hair follicle stem cells for tissue engineering. *Adv. Biomed. Res.* **2016,** *5*.
35. Jacobs, T.; De Geyter, N.; Morent, R.; Desmet, T.; Dubruel, P.; Leys, C., Plasma treatment of polycaprolactone at medium pressure. *Surf. Coat. Technol.* **2011,** *205*, S543-S547.
36. Jacobs, T.; Declercq, H.; De Geyter, N.; Cornelissen, R.; Dubruel, P.; Leys, C.; Morent, R., Improved cell adhesion to flat and porous plasma-treated poly-ε-caprolactone samples. *Surf. Coat. Technol.* **2013,** *232*, 447-455.
37. Dai, R.; Wang, Z.; Samanipour, R.; Koo, K.-i.; Kim, K., Adipose-Derived Stem Cells for Tissue Engineering and Regenerative Medicine Applications. *Stem Cells Int.* **2016,** *2016*, 19.
38. Bunnell, B. A.; Flaat, M.; Gagliardi, C.; Patel, B.; Ripoll, C., Adipose-derived Stem Cells: Isolation, Expansion and Differentiation. *Methods.* **2008,** *45* (2), 115-120.
39. Gimble, J. M.; Katz, A. J.; Bunnell, B. A., Adipose-derived stem cells for regenerative medicine. *Circ.Res.* **2007,** *100* (9), 1249-1260.
40. Ghobeira, R.; Asadian, M.; Vercruysse, C.; Declercq, H.; De Geyter, N.; Morent, R., Wide-ranging diameter scale of random and highly aligned PCL fibers electrospun using controlled working parameters *Polymer.* **2018,** *Under review*.
41. Ko, Y.-M.; Choi, D.-Y.; Jung, S.-C.; Kim, B.-H., Characteristics of plasma treated electrospun polycaprolactone (PCL) nanofiber scaffold for bone tissue engineering. *J. Nanosci. Nanotechnol.* **2015,** *15* (1), 192-195.
42. Yan, D.; Jones, J.; Yuan, X. Y.; Xu, X. H.; Sheng, J.; Lee, J. C. M.; Ma, G. Q.; Yu, Q. S., Plasma treatment of electrospun PCL random nanofiber meshes (NFMs) for biological property improvement. *J. Biomed. Mater. Res. A.* **2013,** *101A* (4), 963-972.
43. Lee, J. C.; Ma, G.; Yu, Q., Plasma treatment of random and aligned electrospun PCL nanofibers. *J. Med. Biol. Eng.* **2013,** *33* (3), 171-178.
44. Cui, W.; Li, X.; Zhou, S.; Weng, J., Degradation patterns and surface wettability of electrospun fibrous mats. *Polym. Degrad. Stabil.* **2008,** *93* (3), 731-738.
45. Deitzel, J. M.; Kosik, W.; McKnight, S. H.; Beck Tan, N. C.; DeSimone, J. M.; Crette, S., Electrospinning of polymer nanofibers with specific surface chemistry. *Polymer.* **2002,** *43* (3), 1025-1029.
46. De Geyter, N.; Morent, R.; Desmet, T.; Trentesaux, M.; Gengembre, L.; Dubruel, P.; Leys, C.; Payen, E., Plasma modification of polylactic acid in a medium pressure DBD. *Surf. Coat. Technol.* **2010,** *204* (20), 3272-3279.
47. Pavliňák, D.; Galmiz, O.; Pavliňáková, V.; Poláček, P.; Kelar, J.; Stupavská, M.; Černák, M., Application of dielectric barrier plasma treatment in the nanofiber processing. *Materials Today Communications* **2018,** *16*, 330-338.
48. Sankar, D.; Shalumon, K.; Chennazhi, K.; Menon, D.; Jayakumar, R., Surface plasma treatment of poly (caprolactone) micro, nano, and multiscale fibrous scaffolds for enhanced osteoconductivity. *Tissue Eng. Part A.* **2014,** *20* (11-12), 1689-1702.
49. Wong, S.-C.; Baji, A.; Leng, S., Effect of fiber diameter on tensile properties of electrospun poly (ε-caprolactone). *Polymer.* **2008,** *49* (21), 4713-4722.

50. Lim, C.; Tan, E.; Ng, S., Effects of crystalline morphology on the tensile properties of electrospun polymer nanofibers. *Appl. Phys. Lett.* **2008,** *92* (14), 141908.
51. Gazzano, M.; Gualandi, C.; Zucchelli, A.; Sui, T.; Korsunsky, A. M.; Reinhard, C.; Focarete, M. L., Structure-morphology correlation in electrospun fibers of semicrystalline polymers by simultaneous synchrotron SAXS-WAXD. *Polymer.* **2015,** *63*, 154-163.
52. Yao, J.; Bastiaansen, C. W.; Peijs, T., High strength and high modulus electrospun nanofibers. *Fibers.* **2014,** *2* (2), 158-186.
53. Richard-Lacroix, M.; Pellerin, C., Molecular orientation in electrospun fibers: from mats to single fibers. *Macromolecules.* **2013,** *46* (24), 9473-9493.
54. Briggs, D., *Surface analysis of polymers by XPS and static SIMS*. Cambridge University Press: 1998.
55. De Geyter, N.; Morent, R.; Leys, C.; Gengembre, L.; Payen, E., Treatment of polymer films with a dielectric barrier discharge in air, helium and argon at medium pressure. *Surf. Coat. Technol.* **2007,** *201* (16-17), 7066-7075.
56. Ahn, H. H.; Lee, I. W.; Lee, H. B.; Kim, M. S., Cellular behavior of human adipose-derived stem cells on wettable gradient polyethylene surfaces. *Int. J. Mol. Sci.* **2014,** *15* (2), 2075-2086.
57. Lee, J. H.; Khang, G.; Lee, J. W.; Lee, H. B., Interaction of different types of cells on polymer surfaces with wettability gradient. *J. Colloid Interface Sci.* **1998,** *205* (2), 323-330.
58. Dolci, L. S.; Quiroga, S. D.; Gherardi, M.; Laurita, R.; Liguori, A.; Sanibondi, P.; Fiorani, A.; Calzà, L.; Colombo, V.; Focarete, M. L., Carboxyl Surface Functionalization of Poly(L-lactic acid) Electrospun Nanofibers through Atmospheric Non-Thermal Plasma Affects Fibroblast Morphology. *Plasma Process. Polym.* **2014,** *11* (3), 203-213.
59. Cho, D.; Chen, S.; Jeong, Y.; Joo, Y. L., Surface hydro-properties of electrospun fiber mats. *Fiber. Polym.* **2015,** *16* (7), 1578-1586.
60. Marmur, A., Soft contact: measurement and interpretation of contact angles. *Soft Matter.* **2006,** *2* (1), 12-17.
61. Milleret, V.; Hefti, T.; Hall, H.; Vogel, V.; Eberli, D., Influence of the fiber diameter and surface roughness of electrospun vascular grafts on blood activation. *Acta. Biomater.* **2012,** *8* (12), 4349-4356.
62. Xu, C.; Yang, F.; Wang, S.; Ramakrishna, S., In vitro study of human vascular endothelial cell function on materials with various surface roughness. *J. Biomed. Mater. Res. A.* **2004,** *71A* (1), 154-161.
63. Kim, H. H.; Kim, M. J.; Ryu, S. J.; Ki, C. S.; Park, Y. H., Effect of fiber diameter on surface morphology, mechanical property, and cell behavior of electrospun poly(ε-caprolactone) mat. *Fiber. Polym.* **2016,** *17* (7), 1033-1042.
64. Morent, R.; De Geyter, N.; Trentesaux, M.; Gengembre, L.; Dubruel, P.; Leys, C.; Payen, E., Influence of discharge atmosphere on the ageing behaviour of plasma-treated polylactic acid. *Plasma Chem. Plasma Process.* **2010,** *30* (4), 525-536.
65. Liu, W.; Zhan, J.; Su, Y.; Wu, T.; Wu, C.; Ramakrishna, S.; Mo, X.; Al-Deyab, S. S.; El-Newehy, M., Effects of plasma treatment to nanofibers on initial cell adhesion and cell morphology. *Colloids Surf. B Biointerfaces.* **2014,** *113*, 101-106.
66. Jahani, H.; Kaviani, S.; Hassanpour-Ezatti, M.; Soleimani, M.; Kaviani, Z.; Zonoubi, Z., The effect of aligned and random electrospun fibrous scaffolds on rat mesenchymal stem cell proliferation. *Yakhteh.* **2012,** *14* (1), 31.
67. Abbasi, N.; Soudi, S.; Hayati-Roodbari, N.; Dodel, M.; Soleimani, M., The effects of plasma treated electrospun nanofibrous poly (ε-caprolactone) scaffolds with different orientations on mouse embryonic stem cell proliferation. *Yakhteh.* **2014,** *16* (3), 245.
68. Prabhakaran, M. P.; Venugopal, J.; Chan, C. K.; Ramakrishna, S., Surface modified electrospun nanofibrous scaffolds for nerve tissue engineering. *Nanotechnology.* **2008,** *19* (45), 455102.
69. Christopherson, G. T.; Song, H.; Mao, H.-Q., The influence of fiber diameter of electrospun substrates on neural stem cell differentiation and proliferation. *Biomaterials.* **2009,** *30* (4), 556-564.